*Mineralogical Magazine* (2021), **85**, 725–743
doi:10.1180/mgm.2021.58

CAMBRIDGE UNIVERSITY PRESS

**Article**

# Microlite-group minerals: tracers of complex post-magmatic evolution in beryl–columbite granitic pegmatites, Maršíkov District, Bohemian Massif, Czech Republic

Štěpán Chládek[1]*, Pavel Uher[2], Milan Novák[3], Peter Bačík[2] and Tomáš Opletal[4]

[1]Department of Geological Engineering, Faculty of Mining and Geology, VŠB – Technical University of Ostrava, 17. listopadu 15, 708 33 Poruba-Ostrava, Czech Republic; [2]Department of Mineralogy, Petrology and Economic Geology, Faculty of Natural Sciences, Comenius University, Ilkovičova 6, 842 15 Bratislava, Slovakia; [3]Department of Geological Sciences, Masaryk University, Kotlářská 2, Brno 611 37, Czech Republic; and [4]Department of Analytical Chemistry, Palacký University, 17. listopadu 12, Olomouc 771 46, Czech Republic

**Abstract**

Microlite-group minerals occur as common replacement products after primary and secondary columbite-group minerals (CGM) in albitised blocky K-feldspar and in coarse-grained, muscovite-rich units of the Schinderhübel I, Scheibengraben and Bienergraben beryl–columbite pegmatites in the Maršíkov District (Silesian Unit, Bohemian Massif, Czech Republic). Textural and compositional variations of microlite-group minerals were examined using electron probe micro-analyses and microRaman spectroscopy (μRS). A complex post-magmatic evolution of the pegmatites and the following microlite populations (Mic) and related processes were found: (1) precipitation of U, Na-rich and F-poor Mic I on cracks in CGM; (2) alteration of Mic I to U-rich together with Na- and F-poor Mic II; and (3) partial replacement of Mic I and II by Mic III with a distinct Na, U and Ti loss and Ca and F gain. Stage (2) includes an extensive leaching of Na, without U loss. The final stage (3) produced euhedral-to-subhedral oscillatory zoned Ca and F enriched Mic III with distinctly different composition to the previous F-poor and *A*-site vacant Mic II. Aggregates of fersmite are associated commonly with Mic III. Distal Mic IIId occurs locally on cracks in K-feldspar or quartz, with compositions analogous to Mic III. Compositional variations and textural features of microlite-group minerals during dissolution–reprecipitation processes serve as sensitive tracers of post-magmatic evolution in granitic pegmatites recording complex interactions between magmatic pegmatite units and externally derived, hydrothermal metamorphic fluids.

**Keywords:** granitic pegmatites, beryl–columbite subtype, Nb–Ta minerals, microlite, columbite, tantalite, fersmite, crystal chemistry, hydrothermal alteration, recrystallisation

(Received 12 January 2021; accepted 9 July 2021; Accepted Manuscript published online: 14 July 2021; Associate Editor: Aniket Chakrabarty)

## Introduction

The pyrochlore-supergroup minerals belong to complex oxide minerals with the general formula $A_{2-m}B_2X_{6-w}Y_{1-n}$ (Atencio *et al.*, 2010; Christy and Atencio, 2013). The *A*-site is occupied by large [8]-coordinated cations: $Na^{+}$, $Ca^{2+}$, $Sr^{2+}$, $Ba^{2+}$, $Fe^{2+}$, $Mn^{2+}$, $Sn^{2+}$, $Pb^{2+}$, $Bi^{3+}$, $Y^{3+}$, $Ce^{3+}$ (+ other rare earth cations), $Sc^{3+}$, $U^{4+}$, $Th^{4+}$, □ (vacancy), or $H_2O$; the *B*-site is filled by [6]-coordinated cations, such as $W^{6+}$, $Nb^{5+}$, $Ta^{5+}$, $Sb^{5+}$, $V^{5+}$, $Ti^{4+}$, $Sn^{4+}$, $Zr^{4+}$, $Hf^{4+}$, $Si^{4+}$, $Al^{3+}$, $Fe^{3+}$ and $Mg^{2+}$; the *X*-site is occupied by anions $O^{2-}$, $OH^{-}$ or $F^{-}$; and the *Y*-site is occupied by anions $O^{2-}$, $OH^{-}$ or $F^{-}$, molecular $H_2O$, □, or very large monovalent cations: $K^{+}$, $Rb^{+}$ and $Cs^{+}$ (Atencio *et al.*, 2010). These minerals are divided according to dominant *B*-site cation occupancy to the classic pyrochlore, microlite and betafite groups (Nb, Ta and Ti dominant), complemented by roméite, elsmoreite, ralstonite and coulsellite groups (Hogarth, 1977; Atencio *et al.*, 2010, 2017).

Members of the pyrochlore and betafite groups occur as magmatic-to-late hydrothermal and supergene or metamorphic accessory components in very diverse geological environments, principally in carbonatites, nepheline syenites and related rocks (e.g. Chakhmouradian and Mitchell, 2002; Melgajero *et al.*, 2012; Walter *et al.*, 2018; Amores-Casals *et al.*, 2020; Dey *et al.*, 2021; Zaitsev *et al.*, 2021), rarely in alkaline and rare-element granites to pegmatites (Johan and Johan, 1994; Lumpkin and Ewing, 1996; De Vito *et al.*, 2006; Prol-Ledesma *et al.*, 2012; Duran *et al.*, 2016; Atencio *et al.*, 2018; Siegel *et al.*, 2018), kimberlites (Sharygin *et al.*, 2009), hydrothermal veins in granite contact aureoles (Lumpkin *et al.*, 2017), or lunar rocks (Meyer and Young, 1988; Mokhov *et al.*, 2008).

In contrast microlite-group minerals form almost exclusively in rare-element granitic pegmatites of the LCT (Li–Ta–Cs) family. They precipitate during various pegmatite stages from late-magmatic/early subsolidus crystallisation associated usually with albitisation, to moderate and low-temperature hydrothermal overprints (e.g. Lumpkin *et al.*, 1986; Černý *et al.*, 1992; Spilde and

*Author for correspondence: Štěpán Chládek, Email: st.chladek@seznam.cz
**Cite this article:** Chládek Š., Uher P., Novák M., Bačík P. and Opletal T. (2021) Microlite-group minerals: tracers of complex post-magmatic evolution in beryl–columbite granitic pegmatites, Maršíkov District, Bohemian Massif, Czech Republic. *Mineralogical Magazine* **85**, 725–743. https://doi.org/10.1180/mgm.2021.58

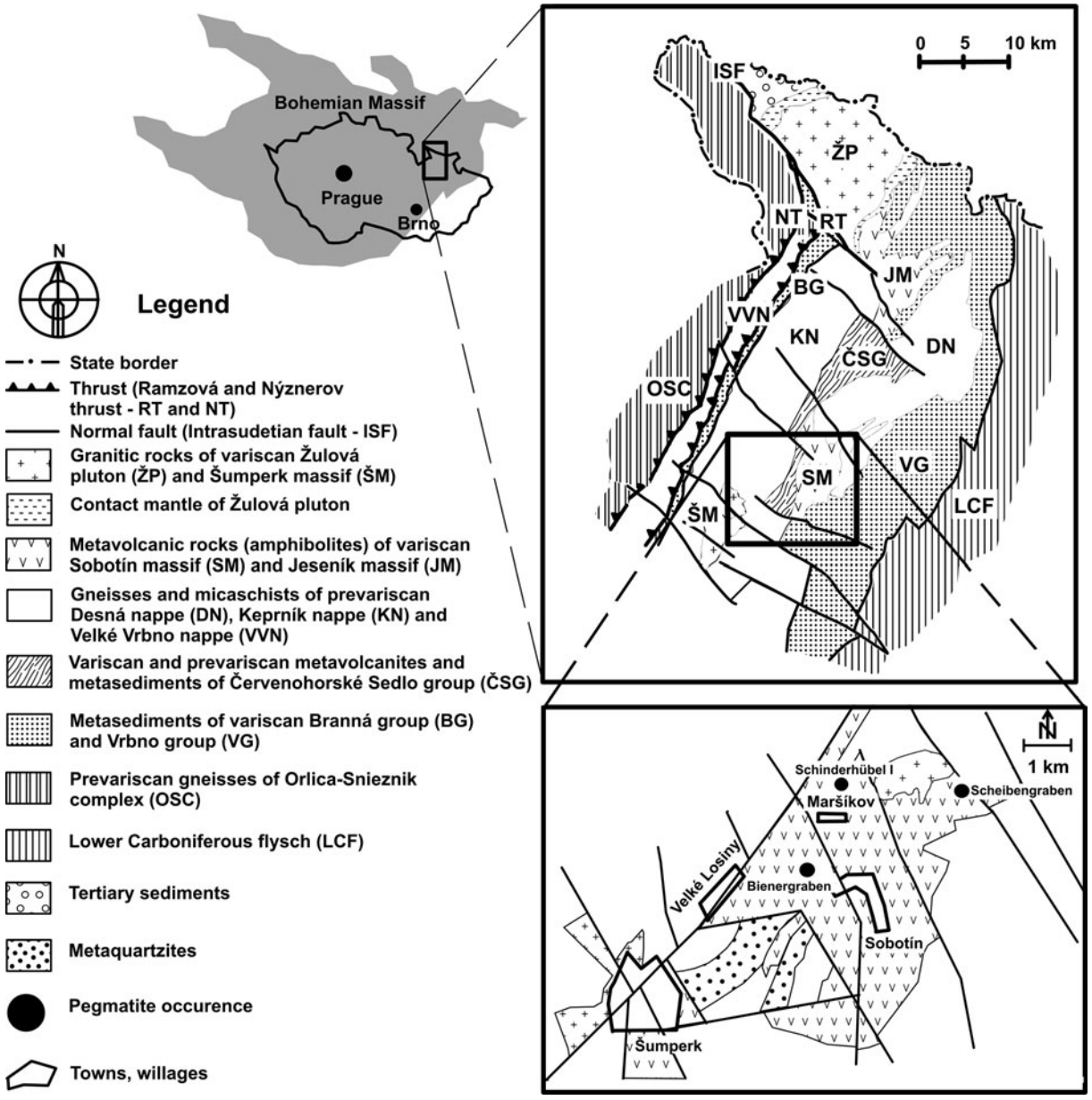


**Fig. 1.** Geological map of the Silesian Domain and the Maršíkov District with individual pegmatite occurrences (modified after Cháb *et al.*, 2007 and on-line map application of the Czech Geological Survey 2019, Chládek *et al.*, 2020).

Shearer, 1992; Lumpkin, 1998; Tindle and Breaks, 1998; Novák and Černý, 1998; Novák *et al.*, 2000, 2003; Guastoni *et al.*, 2008; Chudík *et al.*, 2011; Demartis *et al.*, 2014; Galliski *et al.*, 2016; Szuszkiewicz *et al.*, 2016; Andrade *et al.*, 2017; Loun *et al.*, 2018; Kasatkin *et al.*, 2020). Lumpkin and Ewing (1992) recognised two principal stages of alteration of primary microlite in granitic pegmatites: the first takes place at relatively high temperatures (primary hydrothermal alteration) and is best described by the exchange vectors $^{A}Na^{Y}F^{A}Ca_{-1}{}^{Y}O_{-1}$ and $^{A}\square^{Y}\square^{A}Ca_{-1}{}^{Y}O_{-1}$; the second takes place at relatively low temperature (up to that of subsurface weathering) with $^{A}Na^{Y}F$ $^{A}\square_{-1}{}^{Y}\square_{-1}$, $^{A}Ca^{Y}O$ $^{A}\square_{-1}$ $^{Y}\square_{-1}$ and $^{A}Ca^{X}O$ $^{A}\square_{-1}{}^{X}\square_{-1}$ substitutions. Secondary alteration generates a significant loss of *A*-site elements (especially Na and Ca) and increases *A*-site vacancies and hydration of the mineral (Ewing, 1975; Loun *et al.*, 2018). The precipitation of microlite-group minerals as late-magmatic to post-magmatic (especially hydrothermal) alteration products after primary Nb–Ta phases has been examined in numerous rare-element granitic pegmatites, from less-evolved beryl–columbite–(phosphate) to complex Li–Cs–Ta rich mineralisation where the high activity of volatile elements, such as F, B and P, together with $H_2O$ is typical (e.g. Lumpkin *et al.*, 1986; Tindle and Breaks, 1998; Uher *et al.*, 1998; Chudík *et al.*, 2011; Gonçalves *et al.*, 2019).

We have investigated beryl–columbite pegmatites from the Maršíkov District, Bohemian Massif which are relatively poor in volatile elements (F, B or P). They contain accessory Nb–Ta oxide minerals (maily members of CGM), which have been the object of several investigations (Černý *et al.*, 1992, 1995; Novák *et al.*, 2003; Novák and Dosbaba, 2006; Chládek *et al.*, 2020), though these have had only minor focus on the microlite-group minerals replacing columbite–tantalite. The microlite-group minerals, which can form a variety of textural and compositional types, precipitated

https://doi.org/10.1180/mgm.2021.58 Published online by Cambridge University Press

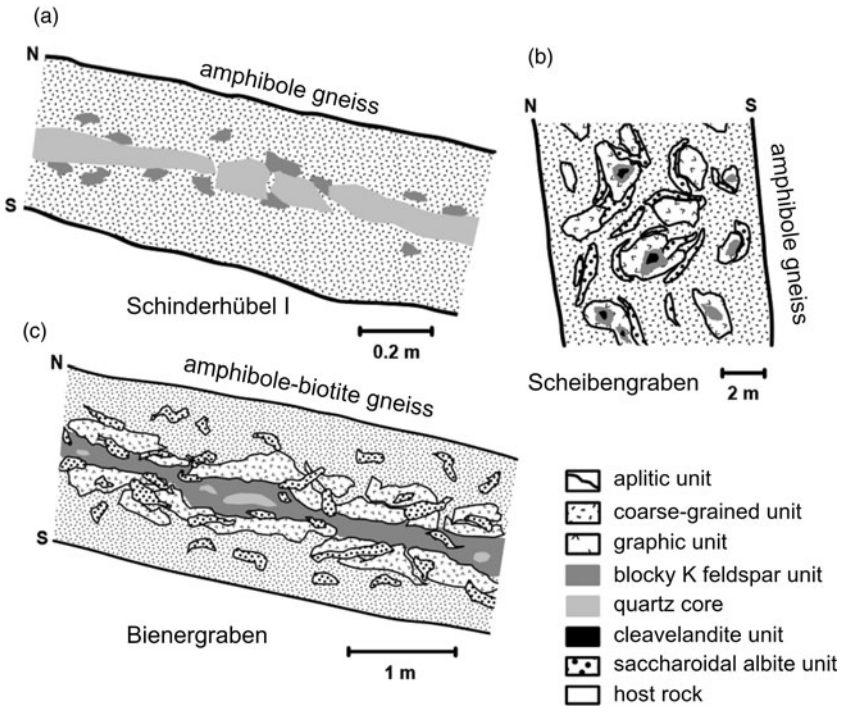


**Fig. 2.** Idealised cross-sections of the pegmatites: (a) Maršíkov – Schinderhübel I (Chládek *et al.*, 2020, modified); (b) Maršíkov – Scheibengraben (Novák *et al.*, 2003, modified); (c) Sobotín – Bienergraben (Chládek *et al.*, 2020, modified).

**Table 1.** EPMA conditions for the Nb–Ta minerals measured.

| Element | Line | Calibrant | CGM d.l. | Mic, Pcl, fersmite d.l. |
|---|---|---|---|---|
| W | *Mβ* | $CaWO_4$ | 1146–1395 | 1208–1427 |
| Nb | *Lα* | $LiNbO_3$ | 611–904 | 635–814 |
| Ta | *Mα* | $LiTaO_3$ | 885–1134 | 990–1281 |
| Si | *Kα* | $ZrSiO_4$ | | 799–868 |
| Ti | *Kα* | $TiO_2$ | 351–477 | 386–526 |
| Sn | *Lα* | $SnO_2$ | | 575–586 |
| Zr | *Lα* | $ZrO_2$ | 621–728 | 606–778 |
| Th | *Mα* | $ThO_2$ | | 540–642 |
| U | *Mα* | $UO_2$ | 756–936 | 733–886 |
| Al | *Kα* | $Al_2O_3$ | | 241–328 |
| Sc | *Kα* | $ScPO_4$ | 369–425 | 342–412 |
| Ce | *Lα* | $CePO_4$ | | 755–856 |
| Y | *Lα* | $YPO_4$ | | 818–1013 |
| Fe | *Kα* | fayalite | 509–571 | 525–630 |
| Mn | *Kα* | rhodonite | 477–553 | 506–621 |
| Mg | *Kα* | forsterite | 219–248 | |
| Ca | *Kα* | wollastonite | | 184–227 |
| Zn | *Kα* | willemite | 649–852 | |
| Na | *Kα* | albite | | 396–626 |
| F | *Kα* | $CaF_2$ | | 537–635 |

d.l. – detection limit = 3σ (in ppm). Mic – microlite; Pcl – pyrochlore.

at least three different stages, which reflect complex subsolidus processes in the host pegmatite. Consequently, the objective of this study is to characterise textural, paragenetic and compositional variations of microlite-group minerals for a better understanding of the complex post-magmatic evolution of the pegmatites.

## Geological setting

The Schinderhübel I, Scheibengraben and Bienergraben beryl–columbite granitic pegmatites are situated near Maršíkov village, Šumperk County in northern Moravia, Czech Republic. These pegmatites are spatially and geologically closely related and belong to the most fractionated bodies of the Maršíkov District. The pegmatites are situated in the southern part of the Neoproterozoic to Devonian Desná Dome (Cháb *et al.*, 1990; Novák and Rejl, 1993; Schulmann *et al.*, 2014), a part of the Silesian Domain, North-East Bohemian Massif (Fig. 1). The Desná Dome consists of crystalline basement including ortho/paragneisses of the Neoproterozoic protolith (570–650 Ma, Kröner *et al.*, 2000) and overlaying Palaeozoic rocks, mainly metaquartzites, metaconglomerates, metapelites and marbles, locally intruded by Middle Devonian (Givetian) (back)-arc affinity metavolcanic rocks of the Sobotín Massif (Janoušek *et al.*, 2014). The Silesian Domain underwent Variscan medium-pressure, Barrovian-type metamorphism at $P \approx 500–700$ MPa and $T \approx 540–650$°C (René, 1983; Cháb *et al.*, 1990; Košuličová and Štípská, 2007).

The Maršíkov District includes several tens of granitic pegmatites of variable size, 1 to 10 m in thickness and up to 100 m in length, forming elongated dykes or slightly irregular lensoid bodies embedded in the host biotite-amphibole gneisses and/or amphibolites of the Sobotín Massif. Radiometric ages of the pegmatites from Maršíkov District and their potential parental granitic source(s) are not known; however, their Variscan Carboniferous age might be analogous to that of pegmatitic leucogranite at Čertovy Kameny hill near Jeseník (334 Ma U–Pb zircon radiometric ages; Hegner and Kröner, 2000), which is also consistent with ages of older granitic plutons: Kłodzko-Złoty Stok, Jawornik, Strzelin, and Kudowa plutons (350–330 Ma, Mikulski *et al.*, 2013) in the adjacent Sudetic block on the North-East margin of the Bohemian Massif in Poland. Younger, late-Variscan, Early Permian magmatic activity documents the granodiorites to granites of the Žulová Pluton with the emplacement age of 292 ± 4 or 291 ± 5 Ma (LA ICP MS U–Pb zircon radiometric age determination; Laurent *et al.*, 2014). Some granitic pegmatites were affected by a metamorphic overprint with local replacement of beryl by chrysoberyl and fibrolitic sillimanite (Dostál, 1966; Franz and Morteani, 1984; Černý *et al.*, 1992). This overprint is

https://doi.org/10.1180/mgm.2021.58 Published online by Cambridge University Press

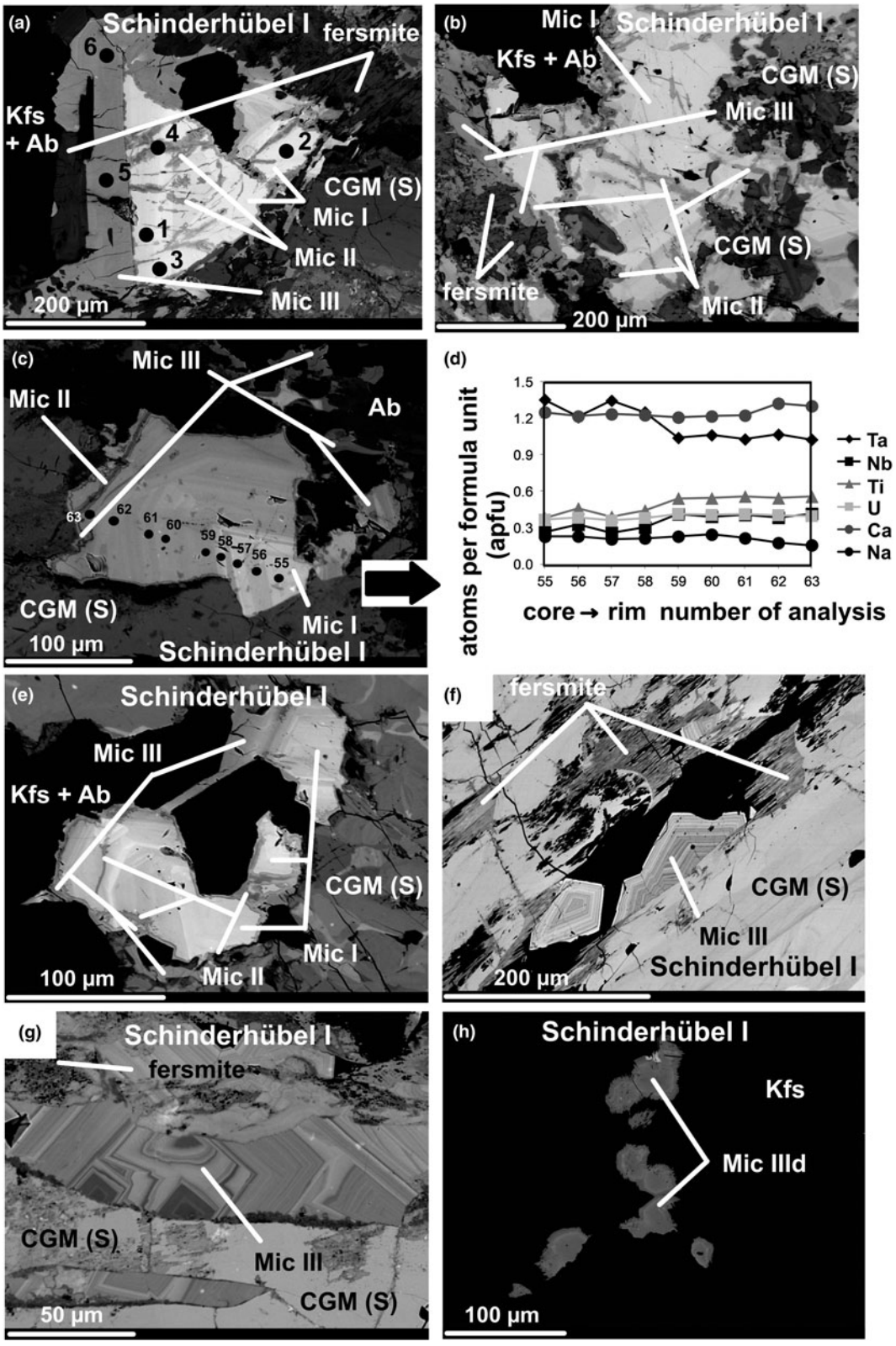


**Fig. 3.** Back-scattered electron (BSE) image of Nb–Ta minerals from the pegmatites: (a) three microlite generations replacing secondary CGM: core domains of Mic I, crosscut by irregularly zoned Mic II, slightly zoned rims of darker Mic III together with tabular fersmite; Raman analysed points: 1–3 Mic I; 4 Mic II; 5 and 6 Mic III (Schinderhübel I); (b) rather homogeneous domains of Mic I characterised by a high porosity and fracturing with irregularly zoned veinlets of Mic II crosscutting Mic I, rims of darker homogeneous Mic III associated with tabular fersmite; microlite types and fersmite replace secondary patchy zoned CGM (Schinderhübel I); (c) oscillatory zoned Mic I with EMPA profile, crosscut by irregularly zoned veinlets of Mic II, rims of indistinctly zoned Mic III; microlite types replace secondary patchy zoned CGM (Schinderhübel I); (d) plot of elemental concentrations in atoms per formula unit (apfu) from core to rim of oscillatory zoned Mic I illustrated in Fig. 3c (Schinderhübel I); (e) oscillatory zoned Mic I crosscut by irregularly zoned veinlets of Mic II, rims of indistinctly zonal Mic III; microlite types replace secondary patchy zoned CGM (Schinderhübel I); (f) oscillatory zoned euhedral Mic III accompanied by tabular dark fersmite on a crack of secondary patchy zoned CGM (Schinderhübel I); (g) oscillatory zoned euhedral Mic III on a crack of secondary patchy zoned CGM (Schinderhübel I); (h) euhedral zoned grains of Mic IIId in crack-fillings in K-feldspar (Schinderhübel I). Abbreviations: Ab – albite, Kfs – K feldspar; CGM (S) – columbite-group minerals (secondary).

https://doi.org/10.1180/mgm.2021.58 Published online by Cambridge University Press

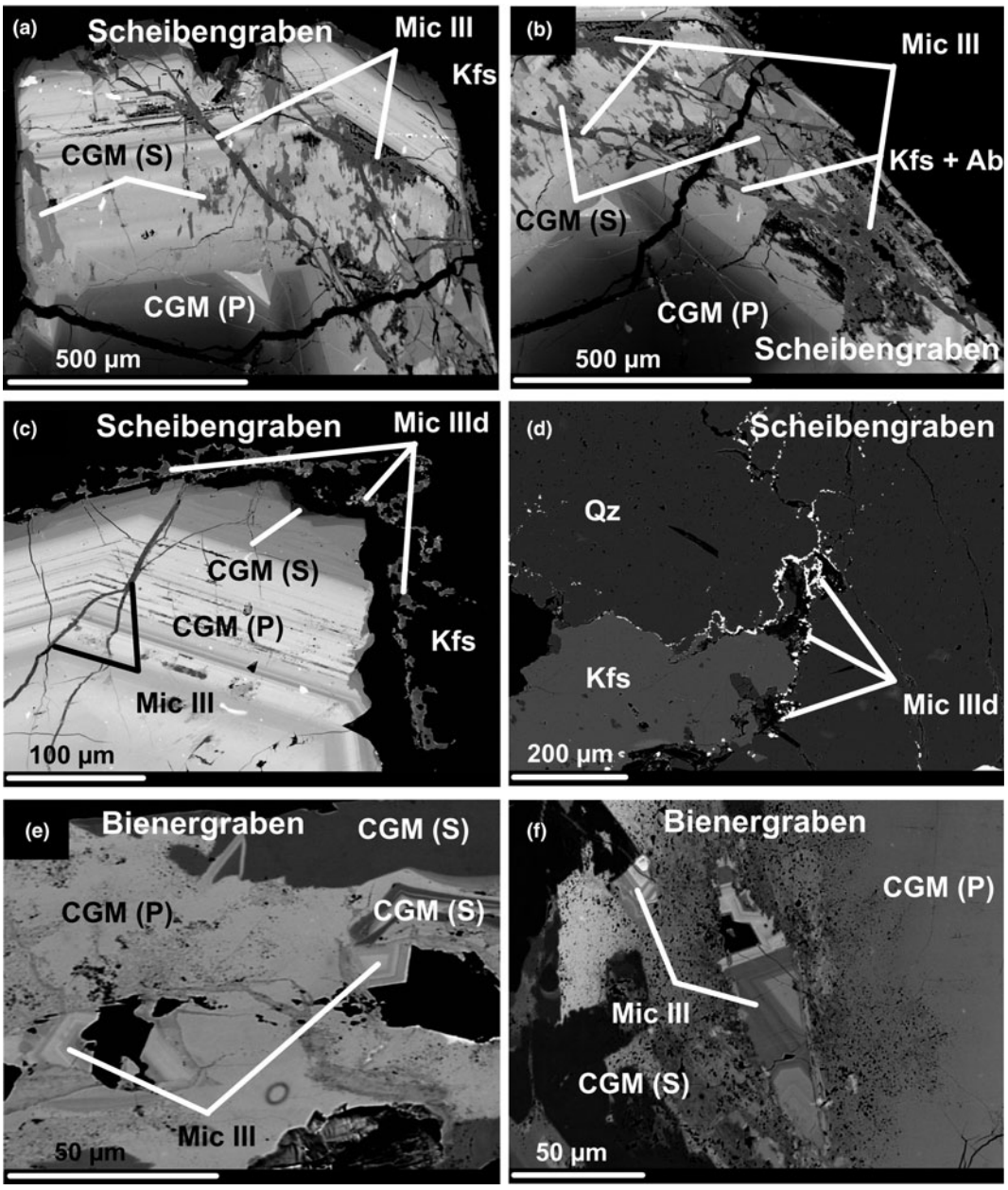


**Fig. 4.** BSE images of Nb–Ta minerals from the pegmatites: (a) veinlets of Mic III crosscutting oscillatory zoned primary CGM replaced by patchy domains of secondary CGM (Scheibengraben); (b) part of the Fig. 4a: veinlets of Mic III crosscutting both oscillatory zoned primary CGM and patchy domains of secondary CGM (Scheibengraben); (c) veinlets of Mic III penetrating oscillatory zoned CGM; Mic IIId chains composed of anhedral grains at the cracks of K-feldspar (Scheibengraben); (d) Mic IIId chains composed of anhedral grains on cracks of K-feldspar and quartz (Scheibengraben); (e) euhedral oscillatory zoned Mic III in vugs and cracks of the primary and secondary CGM (Bienergraben); (f) oscillatory zoned Mic III on cracks of the primary CGM (Bienergraben). Abbreviations: Ab – albite, Kfs – K feldspar; CGM (S) – columbite-group minerals (secondary); CGM (P) – columbite-group minerals (primary).

possibly connected with Upper Carboniferous to Permian (~310–260 Ma) low pressure / high temperature tectono-metamorphic reactivation of the Desná Dome (Schulmann *et al.*, 2014).

## Internal structure, petrography and mineralogy of pegmatites

The granitic pegmatites investigated comprise the following textural-paragenetic units developed from the contact inwards (Fig. 2): (1) an aplitic unit (Kfs + Ab + Qtz + Bt) (≤2 cm thick), evolving to (2) a prevailing coarse-grained, muscovite rich unit (Kfs + Ab + Qtz + Ms). The locally present (3) graphic unit (Kfs + Qtz) gradually evolves into (4) a blocky K-feldspar unit. A quartz core (5) is only developed locally. Small nests of the cleavelandite unit (6) are common in the blocky K-feldspar and coarse-grained unit. Metasomatic replacement of pre-existing units by saccharoidal albite is widespread (Pokorný and Staněk, 1951; Dostál, 1966; Novák *et al.*, 2003).

The Schinderhübel I pegmatite dyke, up to 0.5 m in thickness, consists of a coarse-grained muscovite-rich unit, prevailing over poorly-evolved graphic and blocky K-feldspar units (Fig. 2a). A small quartz core is developed in the central part of this dyke and the albite unit is distributed irregularly within the coarse-grained unit. The metamorphic overprint is relatively weak in

https://doi.org/10.1180/mgm.2021.58 Published online by Cambridge University Press

comparison with the neighbouring strongly foliated chrysoberyl + sillimanite-bearing Schinderhübel III pegmatite (Dostál, 1966; Franz and Morteani, 1984; Černý *et al.*, 1992); however, rare chrysoberyl and sillimanite are present. The largest pegmatite, Scheibengraben (e.g. Pokorný and Staněk, 1951; Novák, 1988; Novák *et al.*, 2003) forms a ~10 m thick lensoid body where the individual pegmatite units are distributed irregularly (Fig. 2b). Saccharoidal albite has extensively replaced the other pegmatite units except for the minor coarse-grained albite (cleavelandite) unit, forming small nests neighbouring blocky K-feldspar. This pegmatite body has only been affected mildly by deformation and metamorphism, mostly along its contacts with the host amphibolite gneiss. The Bienergraben pegmatite (Kruťa, 1966) is a ≤2 m thick dyke characterised by a symmetrically zoned internal structure with common nests of saccharoidal albite and a moderate degree of deformation (Fig. 2c).

All the pegmatites investigated contain very similar mineral assemblages and they correspond to the LCT family and beryl–columbite subtype of rare-element granitic pegmatites (*sensu stricto* Černý and Ercit, 2005). Accessory minerals include common garnet (almandine–spessartine), zircon, fluorapatite, gahnite and uraninite together with other, mostly rare, minerals (Pokorný and Staněk, 1951; Dostál, 1966; Kruťa, 1966; Chládek *et al.*, 2020; Dolníček *et al.*, 2020a,b). Beryl is the only primary magmatic Be mineral together with rare metamorphic chrysoberyl and common secondary bavenite and bohseite. Niobium–tantalum oxide minerals are represented by relatively common columbite–tantalite and microlite, whereas Nb–Ta-rich rutile, titanite, tapiolite-(Fe), rynersonite, and fersmite are less common (Čech, 1973; Černý *et al.*, 1992, 1995; Novák *et al.*, 2003; Novák and Dosbaba, 2006; Chládek *et al.*, 2020). Most granitic pegmatites in the Maršíkov District are relatively poor in B, F and P (Novák, 1988, 2005; Novák *et al.*, 2003), only the most fractionated Scheibengraben body also contains accessory schorl, topaz and triplite (Pokorný and Staněk, 1951).

## Methods

Compositions of Nb–Ta oxide minerals were determined using a Cameca SX100 electron probe micro-analyser (EPMA) in wavelength-dispersion mode at the Dionýz Štúr State Geological Institute, Bratislava; textural patterns were studied in back-scattered electron (BSE) mode using the same apparatus. Measurements were performed with the following analytical conditions: beam diameter of 1−2 μm; an acceleration potential of 15 kV; sample current of 40 nA measured on a Faraday cup; and a counting time of 20 s. Synthetic and natural standards used and detection limits for the individual elements are summarised in Table 1. Concentrations of other measured elements (e.g. Mg, Pb, Zn, Sr, Y, La, Nd, Bi and P) are very low, close to, or below the detection limits of EPMA. Measured data were reduced using the PAP routine (Pouchou and Pichoir, 1985). The structural formulae of columbite-group minerals were normalised on the basis of 24 oxygen atoms and 12 cations using an $Fe^{2+}$ and $Fe^{3+}$ charge-balance calculation according to the procedure of Ercit (1994). The formulae of microlite (Mic) and rare pyrochlore (Pcl) were normalised on the basis of *B*-site cations (W + Ta + Nb + Ti + Si + Zr + Al) = 2 atoms per formula unit (apfu) and by considering that $Sn_{tot}$ is present as $Sn^{2+}$, $Fe_{tot}$ is present as $Fe^{2+}$ and $U_{tot}$ as $U^{4+}$ (Atencio *et al.*, 2010). We also included $Si^{4+}$ and $Al^{3+}$ cations in the sixfold-coordinated *B*-site of the pyrochlore structure following the recent approved nomenclature of pyrochlore-supergroup minerals (Atencio *et al.*, 2010). However, the presence of Si in the pyrochlore

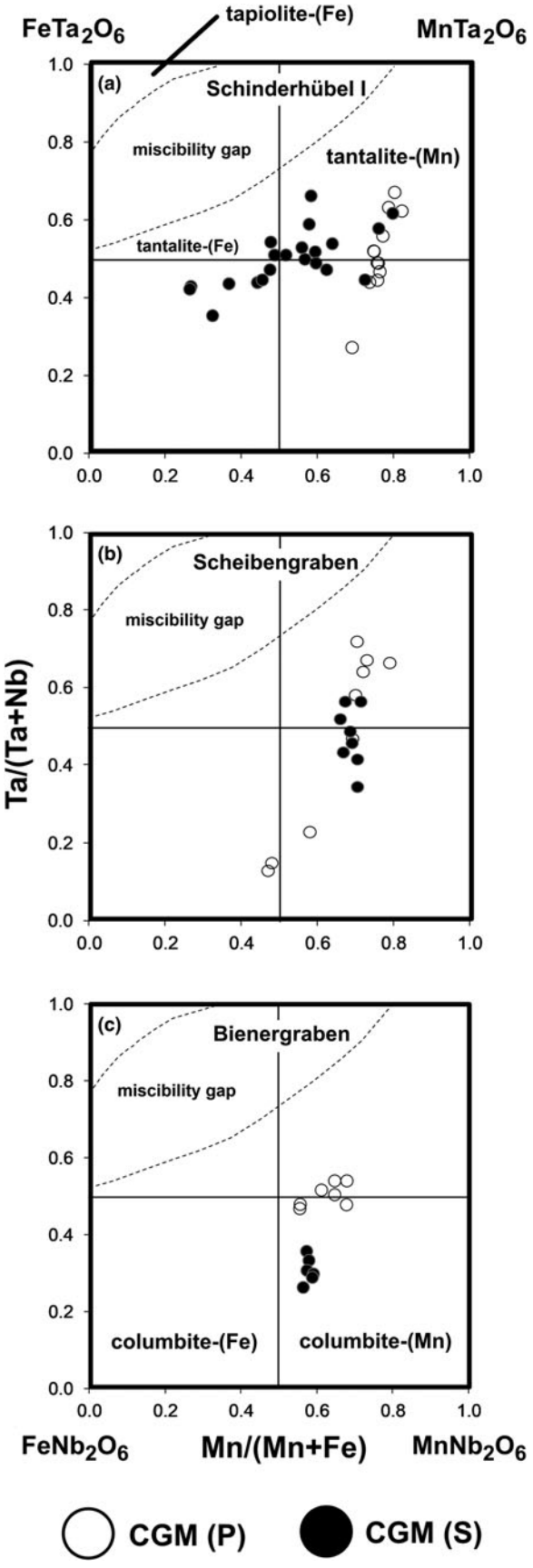


**Fig. 5.** Compositions of primary and secondary CGM in a classification diagram for CGM: (a) Schinderhübel I; (b) Scheibengraben; (c) Bienergraben. Abbreviations: CGM (P) / (S) – primary (magmatic) / secondary (hydrothermal) columbite-group minerals.

https://doi.org/10.1180/mgm.2021.58 Published online by Cambridge University Press

**Table 2.** Representative compositions of primary (P) and secondary (S) CGM from Maršíkov District.*

| Sample | Schl 2 | Schl 2 | Sch 3 | Sch 3 | Bn 1 | Bn 1 |
|---|---|---|---|---|---|---|
| No. anal. (type) | 13 (P) | 15 (S) | 32 (P) | 37 (S) | 18 (P) | 19 (S) |
| Element oxide contents (wt.%) | | | | | | |
| $WO_3$ | 0.06 | 0.14 | 0.65 | 0.26 | 0.07 | 0.12 |
| $Nb_2O_5$ | 35.53 | 30.95 | 32.91 | 34.01 | 33.08 | 50.35 |
| $Ta_2O_5$ | 46.60 | 51.46 | 48.32 | 47.84 | 48.58 | 30.06 |
| $TiO_2$ | 0.20 | 0.31 | 0.43 | 0.39 | 0.89 | 0.79 |
| $ZrO_2$ | 0.15 | – | – | – | 0.21 | – |
| $UO_2$ | 0.10 | 0.07 | 0.07 | 0.07 | 0.10 | 0.14 |
| $Sc_2O_3$ | – | 0.05 | 0.05 | | 0.05 | 0.05 |
| $Fe_2O_3$ | 0.52 | 0.09 | 1.73 | 2.10 | 0.59 | 0.61 |
| FeO | 4.11 | 7.02 | 3.88 | 3.64 | 6.82 | 7.39 |
| MnO | 12.65 | 9.17 | 12.07 | 12.22 | 9.01 | 10.08 |
| MgO | – | 0.21 | – | – | 0.34 | 0.32 |
| ZnO | – | – | – | 0.06 | – | 0.08 |
| Total | 99.91 | 99.49 | 100.12 | 100.59 | 99.74 | 99.99 |
| Element contents in atoms per formula unit (apfu) | | | | | | |
| $W^{6+}$ | 0.004 | 0.010 | 0.047 | 0.018 | 0.005 | 0.008 |
| $Nb^{5+}$ | 4.422 | 3.962 | 4.115 | 4.209 | 4.143 | 5.768 |
| $Ta^{5+}$ | 3.489 | 3.963 | 3.634 | 3.561 | 3.659 | 2.071 |
| $Ti^{4+}$ | 0.041 | 0.066 | 0.089 | 0.080 | 0.185 | 0.151 |
| $Zr^{4+}$ | 0.020 | | | | 0.028 | |
| $U^{4+}$ | 0.006 | 0.004 | 0.004 | 0.004 | 0.006 | 0.008 |
| $Sc^{3+}$ | | 0.012 | 0.012 | | 0.012 | 0.011 |
| $Fe^{3+}$ | 0.108 | 0.018 | 0.361 | 0.434 | 0.122 | 0.115 |
| $Fe^{2+}$ | 0.946 | 1.663 | 0.898 | 0.832 | 1.580 | 1.565 |
| $Mn^{2+}$ | 2.950 | 2.200 | 2.828 | 2.833 | 2.114 | 2.163 |
| $Mg^{2+}$ | | 0.089 | | | 0.140 | 0.121 |
| $Zn^{2+}$ | | | | 0.012 | 0.000 | 0.015 |
| Total cations | 11.986 | 11.987 | 11.988 | 11.983 | 11.994 | 11.996 |
| Total anions | 24.000 | 24.000 | 24.000 | 24.000 | 24.000 | 24.000 |
| Mn/(Mn+Fe) | 0.74 | 0.57 | 0.69 | 0.69 | 0.55 | 0.56 |
| Ta/(Ta+Nb) | 0.44 | 0.50 | 0.47 | 0.46 | 0.47 | 0.26 |
| Total range in individual pegmatites: | | | | | | |
| Pegmatite | Schinderhübel I | | Scheibengraben | | Bienergraben | |
| CGM type | Primary | Secondary | Primary | Secondary | Primary | Secondary |
| Mn/(Mn+Fe) | 0.69–0.82 | 0.26–0.79 | 0.47–0.79 | 0.67–0.71 | 0.55–0.68 | 0.56–0.59 |
| Ta/(Ta+Nb) | 0.27–0.67 | 0.36–0.66 | 0.13–0.72 | 0.34–0.57 | 0.47–0.54 | 0.26–0.36 |

*'–' content of the element is below the detection limit. Abbreviations: Schl — Schinderhübel I, Sch — Scheibengraben, Bn — Bienergraben.

structure (isomorphic constituent or non-structural impurity) remains the subject of controversial discussion (Chakhmouradian and Mitchell, 2002; Bonazzi *et al.*, 2006; Andrade *et al.*, 2013; Dumańska-Słowik *et al.*, 2014). In contrast, $Al^{3+}$ is an essential cation at the *B*-site in hydrokenoralstonite and fluornatrocoulsellite, two recently redefined members of the pyrochlore-supergroup minerals (Atencio *et al.*, 2017). The structural formulae of fersmite were normalised on the basis of 3 cations and 6 oxygen atoms.

The microRaman *in situ* analyses (μRS) were undertaken using a LabRAM-HR Evolution (Horiba Jobin-Yvon) spectrometer system with a Peltier cooled CCD detector and Olympus BX-41 microscope (Department of Geological Sciences, Masaryk University, Brno). A blue diode laser (473 nm) was used to obtain Raman spectra in the range of 50–4000 $cm^{-1}$. The acquisition time was 10 s per frame. The Raman spectra were processed using *PeakFit 4.1.12* (Systat Software, San Jose, CA); absorption bands were fitted by the Lorentz function with automatic background correction and Savitsky-Golay smoothing.

## Results

### *Paragenesis and internal texture of Nb–Ta minerals*

Columbite-group minerals (CGM) were investigated predominantly from the blocky K-feldspar unit in the Scheibengraben and Bienergraben pegmatites and from the muscovite-rich coarse-grained unit in the Schinderhübel I pegmatite. The CGM are common, especially in albitised portions of these two units and are associated closely with muscovite, almandine–spessartine, gahnite, zircon, beryl, fluorapatite and uraninite. Primary magmatic oscillatory zoning of CGM is commonly developed and is replaced locally by convolute oscillatory zoned-to-patchy domains of secondary (early hydrothermal) CGM (Figs 3, 4; Chládek *et al.*, 2020).

Two principal textural types of microlite (pyrochlore) were distinguished in the sense of Novák *et al.* (2015): a proximal microlite directly replacing the CGM, commonly along cracks; and a near distal type that forms aggregates of small grains within cracks in host K-feldspar and quartz, close to grains of replaced CGM (Figs 3, 4). The detailed textural relationships and compositional variations at the individual pegmatites show four distinct types of microlite- and rarely, pyrochlore-group minerals. Proximal Mic I to Mic III replace both primary and secondary CGM (Figs 3, 4), whereas early Mic I and II are replaced by late Mic III; and by distal Mic IIId in cracks of host K-feldspar and quartz. Only the Schinderhübel I pegmatite contained all the types of microlite described (Fig. 3a–h).

Microlite I forms subhedral grains replacing primary and secondary CGM along fractures (Fig. 3a–c, e); it constitutes homogeneous (Fig. 3a,b) to oscillatory zoned (Fig. 3c,e) corroded domains, characterised by indistinct compositional zonation

https://doi.org/10.1180/mgm.2021.58 Published online by Cambridge University Press

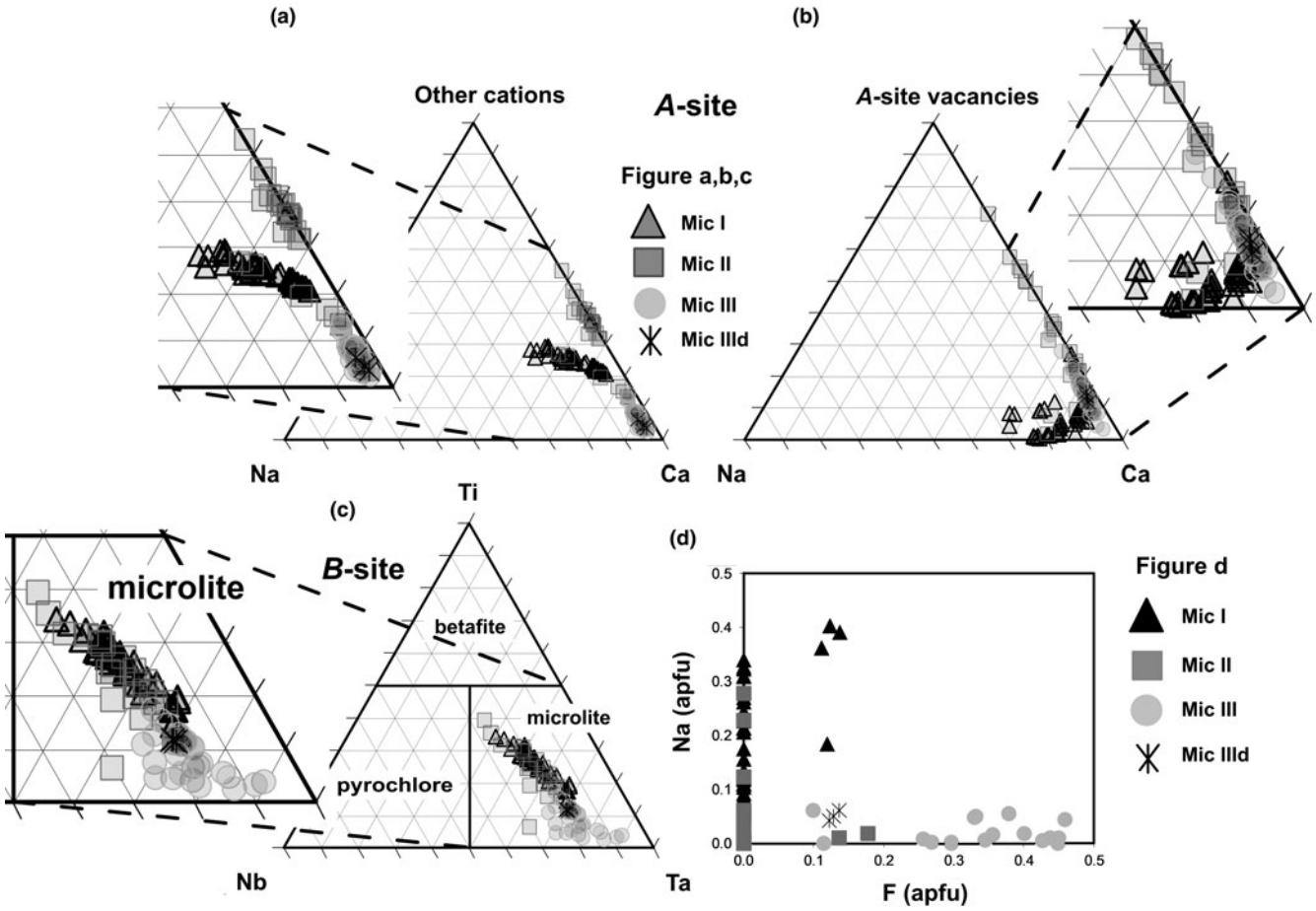


**Fig. 6.** Ternary classification diagrams and F–Na plot for microlites in Schinderhübel I: (a) *A*-site (Na–Ca–Other cations); (b) *A*-site (Na–Ca–vacancy); (c) *B*-site (Nb–Ta–Ti); (d) F *vs*. Na plot; note, 'Other cations' represent Th, Sb, Sc, Ce, Fe, Mn and Sn in the *A*-site.

(Fig. 3d). Microlite I is cut and replaced locally by irregularly zoned veinlets of Mic II (Fig. 3a–c, e). Microlite III forms late rims and homogeneous to slightly oscillatory zoned euhedral-to-subhedral grains surrounding and replacing Mic I–II (Fig. 3a–c, e) and CGM in cracks (Fig. 3f,g). Microlite III is associated locally with fibrous aggregates of fersmite (Fig. 3a,b,f,g). Thin chains composed of euhedral-to-anhedral grains of distal microlite IIId (Mic IIId) were identified occasionally on cracks in K-feldspar grains close to CGM (≤300 μm, Fig. 3h). Relatively homogeneous Mic III veinlets (≤1 mm in length) commonly crosscut CGM crystals (Fig. 4a–c) at Scheibengraben. Distal Mic IIId forms anhedral grains grouped into chains in cracks in quartz and K-feldspar close to CGM (Fig. 4c,d). At Bienergraben, similar to Mic III from Schinderhübel I, oscillatory-to-homogeneous euhedral-to-subhedral Mic III fills cavities and occurs in cracks in CGM (Fig. 4e,f),

## Composition

### *Columbite–tantalite*

Both primary magmatic and secondary CGM are characterised by variable evolution in one or both Mn/(Mn+Fe) and Ta/(Ta+Nb) ratios from columbite-(Fe) to tantalite-(Mn) (Fig. 5; Table 2; Chládek *et al.*, 2020). In the Schinderhübel I pegmatite, secondary CGM are compositionally more variable than primary CGM, the opposite to their behaviour at Scheibengraben (compare with Fig. 5a,b). Primary and secondary compositions are poor in minor elements except for Ti (≤2.0 wt.% $TiO_2$) and Mg (≤0.6 wt.% MgO) in secondary CGM from Schinderhübel I. Calculated $Fe^{3+}$ values are up to 3.0 wt.% $Fe_2O_3$ in both primary and secondary CGM (Table 2).

### *Microlite- and pyrochlore-group minerals*

In the Schinderhübel I pegmatite (Fig. 6; Table 3), Ca (≤1.76 apfu) is typically the dominant cation in the *A*-site of most of the microlite compositions (Fig. 6a,b). The contents of Na and U decrease from Mic I (≤0.40 apfu Na, ≤0.48 apfu U) through Mic II (≤0.28 apfu Na, ≤0.47 apfu U) to Mic III (≤0.09 apfu Na, ≤0.10 apfu U) and Mic IIId (≤0.06 apfu Na, ≤0.01 apfu U). The Ta/(Ta+Nb) ratio is similar in Mic I (0.61–0.84) and Mic II (0.57–0.81); increases in Mic III (0.74–0.93), and is slightly higher in Mic IIId (0.79–0.81). However, concentrations of Ti decrease in the same manner from Mic I and Mic II (≤0.68 apfu and ≤0.78 apfu) to Mic III (≤0.35 apfu) and Mic IIId (≤0.24 apfu, Fig. 6c). Trace concentrations of Si (≤0.01 apfu), Zr (≤0.02 apfu) are present in Mic III and Mic IIId (Table 3), whereas W and Nb are more-or-less constant in all microlite types (Table 3). Microlite III is distinctly enriched in F (≤0.47 apfu) compared to Mic I (≤0.14 apfu), Mic II (≤0.18 apfu) and also Mic IIId (≤0.14 apfu, Fig. 6d; Table 3). The associated fersmite has a

https://doi.org/10.1180/mgm.2021.58 Published online by Cambridge University Press

**Table 3.** Representative compositions of microlite (Mic) from Schinderhübel I.*

| Sample | Schl 2 | Schl 4 | Schl 3 | Schl 2 | Schl 26 | Schl 3 | Schl 2 | Schl 2 |
|---|---|---|---|---|---|---|---|---|
| No. anal. (type) | 27 (Mic I) | 29 (Mic I) | 3 (Mic II) | 4 (Mic II) | 5 (Mic III) | 17 (Mic III) | 35 (Mic IIId) | 36 (Mic IIId) |
| Element oxide contents (wt.%) | | | | | | | | |
| $WO_3$ | 0.24 | 0.35 | 0.33 | 0.19 | – | – | 0.05 | 0.16 |
| $Nb_2O_5$ | 9.30 | 9.80 | 9.85 | 9.76 | 8.77 | 9.47 | 9.26 | 9.46 |
| $Ta_2O_5$ | 44.95 | 42.90 | 49.67 | 49.41 | 63.89 | 62.49 | 63.02 | 62.68 |
| $SiO_2$ | – | – | – | – | 1.02 | 1.26 | – | – |
| $TiO_2$ | 7.99 | 9.00 | 8.92 | 5.82 | 4.15 | 3.55 | 3.64 | 3.75 |
| $ZrO_2$ | – | – | – | – | 0.16 | 0.19 | 0.11 | 0.10 |
| $ThO_2$ | 0.10 | 0.12 | 0.12 | 0.17 | – | 0.32 | – | – |
| $UO_2$ | 21.05 | 22.52 | 21.03 | 15.04 | 0.73 | 0.55 | 0.25 | 0.55 |
| $Al_2O_3$ | 0.10 | – | 0.09 | – | 0.07 | 0.14 | 0.13 | – |
| $Sc_2O_3$ | – | – | – | – | – | 0.06 | 0.05 | – |
| $Ce_2O_3$ | 0.11 | – | 0.12 | 0.13 | – | | 0.13 | 0.15 |
| FeO | 0.18 | 0.25 | 0.40 | 0.25 | 0.14 | 0.30 | 0.63 | 0.37 |
| MnO | 0.06 | 0.07 | 0.27 | 0.17 | 0.36 | 0.29 | 0.08 | 0.10 |
| SnO | 0.07 | 0.07 | 0.05 | – | – | – | – | – |
| CaO | 11.96 | 11.99 | 7.37 | 14.16 | 18.35 | 18.29 | 18.18 | 18.24 |
| $Na_2O$ | 1.57 | 1.55 | 0.10 | 0.71 | 0.22 | 0.39 | 0.38 | 0.32 |
| $F^-$ | – | – | – | – | 1.55 | 1.74 | 0.52 | 0.49 |
| $-O=F_2$ | – | – | – | – | -0.65 | -0.73 | -0.22 | -0.21 |
| Total | 97.69 | 98.63 | 98.32 | 95.80 | 98.76 | 98.31 | 96.22 | 96.16 |
| Element contents in atoms per formula unit (apfu) | | | | | | | | |
| $Th^{4+}$ | 0.002 | 0.002 | 0.002 | 0.003 | | 0.006 | | |
| $U^{4+}$ | 0.414 | 0.437 | 0.376 | 0.300 | 0.013 | 0.010 | 0.005 | 0.010 |
| $Sc^{3+}$ | | | | | | 0.004 | 0.004 | |
| $Ce^{3+}$ | 0.004 | 0.003 | 0.004 | 0.004 | | | 0.004 | 0.004 |
| $Fe^{2+}$ | 0.013 | 0.036 | 0.027 | 0.037 | 0.009 | 0.020 | 0.043 | 0.052 |
| $Mn^{2+}$ | 0.004 | 0.005 | 0.018 | 0.013 | 0.024 | 0.019 | 0.006 | 0.007 |
| $Sn^{2+}$ | 0.003 | 0.003 | 0.002 | | | | | |
| $Ca^{2+}$ | 1.133 | 1.119 | 0.635 | 1.362 | 1.534 | 1.539 | 1.604 | 1.613 |
| $Na^+$ | 0.269 | 0.262 | 0.016 | 0.123 | 0.033 | 0.059 | 0.061 | 0.050 |
| Total *A* | 1.842 | 1.867 | 1.080 | 1.842 | 1.613 | 1.657 | 1.727 | 1.736 |
| $W^{6+}$ | 0.005 | 0.008 | 0.007 | 0.004 | | | 0.001 | 0.003 |
| $Nb^{5+}$ | 0.372 | 0.386 | 0.358 | 0.396 | 0.309 | 0.336 | 0.345 | 0.353 |
| $Ta^{5+}$ | 1.081 | 1.016 | 1.087 | 1.206 | 1.355 | 1.335 | 1.412 | 1.407 |
| $Si^{4+}$ | | | | | 0.080 | 0.099 | | |
| $Ti^{4+}$ | 0.531 | 0.590 | 0.540 | 0.393 | 0.243 | 0.210 | 0.226 | 0.233 |
| $Zr^{4+}$ | | | | | 0.006 | 0.007 | 0.004 | 0.004 |
| $Al^{3+}$ | 0.010 | | 0.010 | | 0.006 | 0.013 | 0.013 | |
| Total *B* | 1.999 | 2.000 | 2.002 | 1.999 | 1.999 | 2.000 | 2.001 | 2.000 |
| $F^-$ | | | | | 0.382 | 0.432 | 0.135 | 0.128 |
| $O^{2-}$ | 6.853 | 6.881 | 6.178 | 6.895 | 6.246 | 6.258 | 6.509 | 6.544 |
| Total cations | 3.841 | 3.867 | 3.082 | 3.841 | 3.612 | 3.657 | 3.728 | 3.736 |
| Total anions | 6.853 | 6.881 | 6.178 | 6.895 | 6.628 | 6.690 | 6.644 | 6.672 |
| Nb# | 18.8 | 19.4 | 18.0 | 19.8 | 16.2 | 17.9 | 17.4 | 17.7 |
| Ta# | 54.5 | 51.0 | 54.8 | 60.5 | 71.1 | 71.0 | 71.2 | 70.6 |
| Ti# | 26.8 | 29.6 | 27.2 | 19.7 | 12.7 | 11.2 | 11.4 | 11.7 |
| Ta/(Ta+Nb) | 0.74 | 0.72 | 0.75 | 0.75 | 0.81 | 0.80 | 0.80 | 0.80 |

*'–' content of the element is below detection limit. Abbreviations: Schl – Schinderhübel I; *A*, *B* – structural positions of pyrochlore structure; Mic I, II, III, IIId – microlite types. End-members of pyrochlore-supergroup minerals (molecule %): pyrochlore (Nb#), microlite (Ta#) and betafite (Ti#).

relatively low Ta/(Ta+Nb) ratio (0.11–0.43) in comparison with Mic I–III, ~1.0 apfu Ca and minor contents of REE and U (Table 4).

At Scheibengraben, Mic III and IIId (Fig. 4a–d) are similar to Mic III from Schinderhübel I (Figs 6, 7; Table 5), only concentrations of Na are slightly higher (≤0.32 apfu) and locally also Si (≤0.33 apfu, Table 5). Euhedral-to-subhedral oscillatory zoned Mic III from Bienergraben is similar to Mic III and IIId in Schinderhübel I and Scheibengraben (Figs 6–8; Table 5); however, it differs in having a greater variation in Ta/(Ta+Nb) = 0.44–0.94 (Fig. 8a–c; Table 5).

The compositions investigated belong to the microlite group, with fewer examples belonging to the pyrochlore group at the Bienergraben pegmatite, with Ca cations dominant in the *A*-site (Figs 6–8; Tables 3 and 5). Analytical totals (91.0 to 98.6 wt.%), as well as total O (6.03–6.90 apfu) and F (0.00–0.43 apfu) indicate the presence of oxycalciomicrolite, fluorcalciomicrolite and hydroxycalciomicrolite. However, some compositons might represent zero-valence dominant members at the *A*- and *Y*-sites (Atencio *et al.*, 2010).

Compositional trends in the individual types of microlite from the Schinderhübel I pegmatite were examined in detail and correlations between the individual elements and *A*-site vacancy are illustrated in Fig. 9. An inverse correlation between Ca and Na at Mic I (Fig. 9a), and only trace concentrations of F in most compositions (Fig. 9b) suggest the dominant substitution is (1): $^{A}Na^{Y}(OH)^{A}Ca_{-1}{}^{Y}O_{-1}$. The correlation vectors between U and Ti at ~0.5 (Fig. 9c), Ti/(Nb+Ta) ≈ –1 (Fig. 6c) and the *A*-site vacancy *versus* U close to –1 (Fig. 9d) can be expressed *via* substitution (2): $^{A}U_{0.5}{}^{B}Ti^{Y}O^{A}\square_{-0.5}{}^{B}(Ta,Nb)_{-1}{}^{Y}(OH)_{-1}$. Uranium was considered as $U^{4+}$ although $U^{6+}$ as the uranyl group $(UO_2)^{2+}$ has also been

https://doi.org/10.1180/mgm.2021.58 Published online by Cambridge University Press

**Table 4.** Representative compositions of fersmite from Schinderhübel I.*

| Sample | Schl 2 | Schl 2 | Schl 18 | Schl 5 |
|---|---|---|---|---|
| Anal. (type) | 11 | 14 | 24 | 74 |
| Element oxide contents (wt.%) | | | | |
| $WO_3$ | 0.05 | 0.04 | 0.11 | 0.08 |
| $Nb_2O_5$ | 42.65 | 39.66 | 52.03 | 45.52 |
| $Ta_2O_5$ | 38.03 | 39.25 | 28.63 | 35.89 |
| $SiO_2$ | – | – | 0.13 | – |
| $TiO_2$ | 2.77 | 2.77 | 1.80 | 1.02 |
| $ZrO_2$ | – | – | 0.06 | – |
| $UO_2$ | 0.11 | 0.11 | 0.07 | 0.09 |
| $Sc_2O_3$ | 0.05 | 0.05 | 0.05 | 0.00 |
| $Y_2O_3$ | – | – | 0.16 | – |
| $Ce_2O_3$ | 0.15 | 0.02 | – | 0.20 |
| FeO | 0.29 | 0.12 | 0.26 | 0.02 |
| MnO | 0.09 | 0.06 | 0.15 | 0.10 |
| CaO | 15.24 | 14.98 | 15.59 | 14.81 |
| $F^-$ | – | – | 0.37 | – |
| Total | 99.43 | 97.06 | 99.42 | 97.74 |
| Element contents in atoms per formula unit (apfu) | | | | |
| $W^{6+}$ | 0.001 | 0.001 | 0.002 | 0.001 |
| $Nb^{5+}$ | 1.216 | 1.169 | 1.447 | 1.320 |
| $Ta^{5+}$ | 0.652 | 0.696 | 0.465 | 0.626 |
| $Si^{4+}$ | | | 0.008 | |
| $Ti^{4+}$ | 0.131 | 0.136 | 0.084 | 0.049 |
| $Zr^{4+}$ | | | 0.002 | |
| $U^{4+}$ | 0.002 | 0.002 | 0.001 | 0.001 |
| $Sc^{3+}$ | 0.003 | 0.003 | 0.003 | 0.000 |
| $Y^{3+}$ | | | 0.005 | |
| $Ce^{3+}$ | 0.003 | 0.000 | 0.000 | 0.005 |
| $Fe^{2+}$ | 0.015 | 0.007 | 0.014 | 0.001 |
| $Mn^{2+}$ | 0.005 | 0.003 | 0.008 | 0.005 |
| $Ca^{2+}$ | 1.030 | 1.046 | 1.035 | 1.018 |
| $F^-$ | | | 0.071 | |
| $O^{2-}$ | 6.000 | 6.000 | 6.075 | 6.000 |
| Total cations | 3.058 | 3.063 | 3.074 | 3.026 |
| Total anions | 6.000 | 6.000 | 6.075 | 6.000 |
| Ta/(Ta+Nb) | 0.35 | 0.37 | 0.24 | 0.32 |

*'–' content of the element is below the detection limit. Abbreviations: Schl — Schinderhübel I.

found in microlite, for example from the Harding pegmatite (Lumpkin *et al.*, 1986). However, substitution 2 has only minor importance and these data are not as conclusive as for substitution (1). The compositions of Mic II show an inverse correlation between the *A*-site vacancy and Ca (Fig. 9e) and trace concentrations of Na (Fig. 9a). These data suggest substitution (3): $^{A}Ca^{Y}O^{A}\square_{-1}{}^{Y}\square_{-1}$; however, these data are less conclusive, mainly due to the more heterogeneous composition of Mic II (Fig. 6a,b). The very unusual composition of Mic III (+ IIId) can be expressed by substitution (4): $^{A}Ca_{0.5}{}^{Y}F_{0.5}{}^{Y}(OH)_{0.5}\ {}^{A}\square_{-0.5}{}^{Y}\square_{-1}$ as there is a positive correlation for Ca *versus* F (Fig. 9b), an almost total absence of Na, and low contents of Ti and U (Fig. 9a,c,f).

### *Raman spectrometry*

Raman spectra of Mic I–III from the Schinderhübel I pegmatite display very broad bands with large full width at half maximum (FWHM) and extensive overlaps (Fig. 10a). These bands can be attributed to specific modes according to Geisler *et al.* (2004) (Fig. 10; Table 6): (a) $T_{2g}$ modes in the region of 196–259 $cm^{-1}$ assigned to *A*–*Y* stretching and *X*–*A*–*Y* bending and the 637–802 $cm^{-1}$ region for *B*–*X* octahedra stretching, and two types of band with ambiguous assignment but probably forbidden or combination mode and vibrational mode in an amorphous structure; (b) $E_g$ modes between 286 and 328 $cm^{-1}$ assigned to *X*–*B*–*X* bending; (c) $A_{1g}$ modes in the region of 532–540 $cm^{-1}$ assigned to *B*–*X* octahedra stretching. Features such as the large FWHM, overlapping bands and the highest intensity of the 773–802 $cm^{-1}$ bands probably associated with a vibrational mode in an amorphous structure, indicate the low-ordered crystalline to amorphous state of the microlites investigated. The presence of low-intensity $(OH)^-$ bands was observed only in two spectra of Mic I (Fig. 10b; Table 6, spectrum 2) and III (Fig. 10b; Table 6, spectrum 5). All spectra display variable but relatively intensive luminescence resulting in the increased background.

## Discussion

### *Compositional variability of microlite*

Proximal microlites from the Schinderhübel I pegmatite demonstrate the evolution from Mic I, with high Na, moderate Ca and low *A*-site vacancy, to Mic II characterised by low Na, variable *A*-site vacancy and slightly elevated Ca (Fig. 6; Table 3); both have high but variable U and very low contents of F. The Ta/(Ta+Nb) ratio is relatively constant whereas Ti is variable in both types. Compared to Mic I and II, Mic III differs significantly in having higher Ca, low *A*-site vacancy, higher Ta/(Ta+Nb), lower Ti and generally with high, but variable F. The distal Mic IIId is generally similar to Mic III, it differs only in fewer compositional variations, perhaps due to fewer analysed spots.

Oxygen is a dominant anion in the compositions with high totals (Tables 3, 5). Molecular water was not determined using μRS, only the local occurrence of a hydroxyl anion in the *Y*-site of Mic I and III was indicated (Fig. 10; Table 6). Hence, mutual relationships between Na and Ca *vs.* F (Figs 6–9) in Mic I–III (+ IIId) illustrate different compositional trends in these sites. In the Schinderhübel I pegmatite, two distinct trends are evident (Fig. 6d), although both differ from data commonly published (e.g. Lumpkin *et al.*, 1986; Loun *et al.*, 2018). Microlite I with elevated Na content and Na-poor Mic II have low to zero concentrations of F (Fig. 6d; Table 3). However, Mic III (+ IIId) is F-enriched and Na-poor. Such a trend is remarkable because secondary microlites typically contain only minor to zero F concentrations and the *A*-site has a large vacancy content (e.g. Lumpkin *et al.*, 1986; Lumpkin and Ewing, 1992; Loun *et al.*, 2018). Although an unusual trend it has been documented in post-magmatic microlite from beryl–columbite pegmatites of the Western Carpathians, which contain almost 3 wt.% F (≤0.9 apfu F) and ≤3.5 wt.% $Na_2O$ (≤0.6 apfu Na, Chudík and Uher, 2009; Chudík *et al.*, 2011) and similar microlite has also been described from the Schinderhübel I pegmatite (Černý *et al.*, 1992). A reduction in analytical totals could be explained by an incorporation of hydroxyl groups $(OH)^-$ into the microlite structure or the presence of water molecules in domains of higher porosity (Geisler *et al.*, 2004). This phenomenon is also known from altered zircon and monazite characterised by extensive porosity (Lee and Tromp, 1995; Nasdala *et al.*, 2009). Unaltered domains of Mic I and the majority of Mic III have analytical totals ≈99 wt.%, which decreases to ≈91 wt.% for more altered domains, mainly in Mic II (Figs 6–8; Tables 3, 5).

The substitution mechanisms in the individual types of microlite from the Schinderhübel I pegmatite differ significantly. The dominant substitution (1) $^{A}Na^{Y}(OH)^{A}Ca_{-1}{}^{Y}O_{-1}$ in the heterogeneous Mic I is well constrained, whereas the minor substitution (2) $^{A}U_{0.5}{}^{B}Ti^{Y}O^{A}\square_{-0.5}{}^{B}(Ta,Nb)_{-1}{}^{Y}(OH)_{-1}$, illustrating variations in Ti and (Nb, Ta)$^{5+}$, is less pronounced. Substitution (1) is similar to the substitution $^{A}Na^{Y}F^{A}Ca_{-1}{}^{Y}O_{-1}$ interpreted in numerous pegmatites as primary hydrothermal alteration (Lumpkin *et al.*, 1986;

https://doi.org/10.1180/mgm.2021.58 Published online by Cambridge University Press

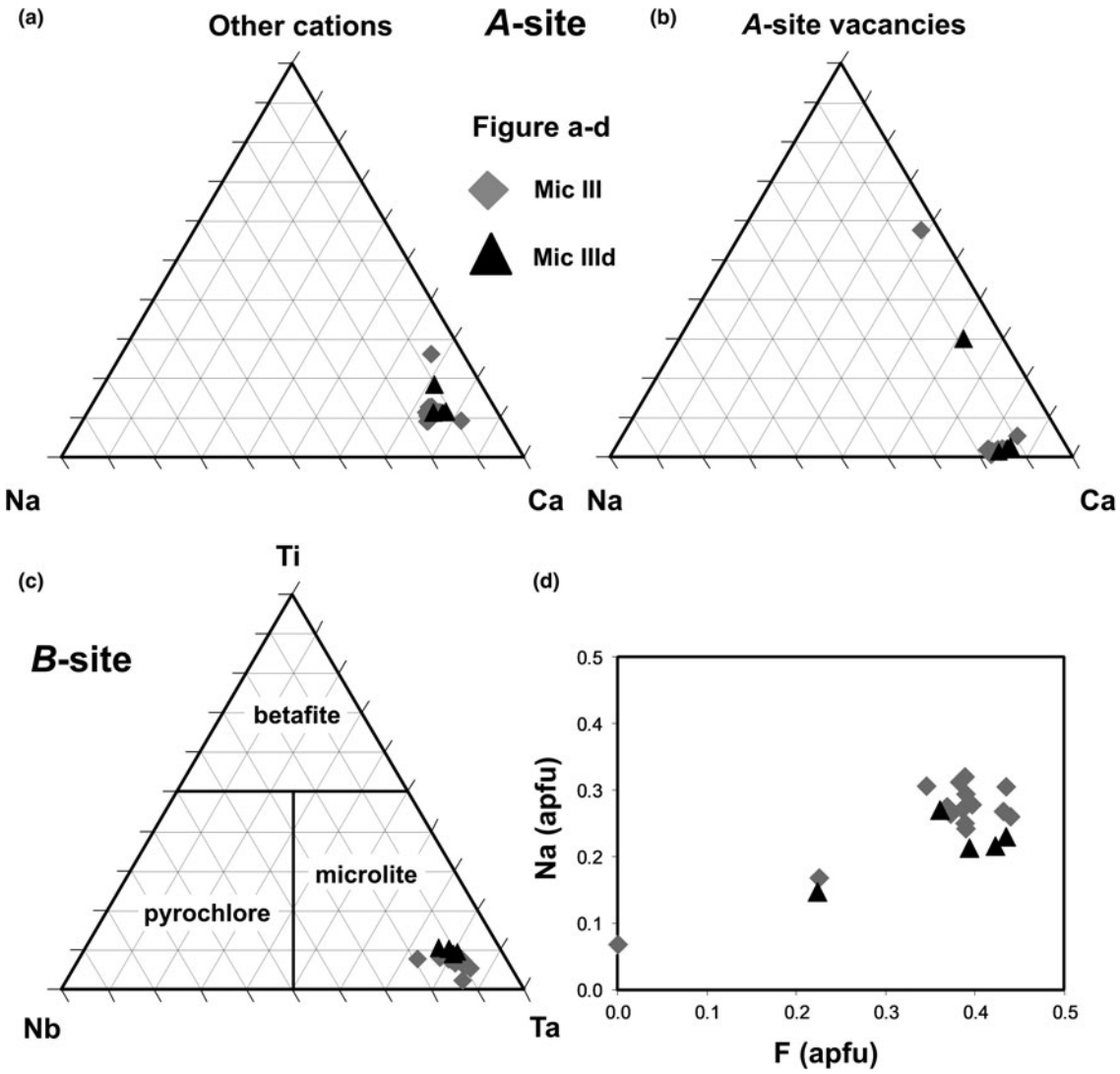


**Fig. 7.** Ternary classification diagrams and F–Na plot for microlites in Scheibengraben: (a) *A*-site (Na–Ca–Other cations); (b) *A*-site (Na–Ca–vacancy); (c) *B*-site (Nb–Ta–Ti); (d) F *vs.* Na plot; note 'Other cations' represent Th, Sb, Sc, Ce, Fe, Mn and Sn in the *A*-site.

Lumpkin and Ewing, 1992; Novák and Černý, 1998). However, microlite I is F-poor, hence this substitution has been modified to the F-free substitution (1) $^{A}Na^{Y}(OH)^{A}Ca_{-1}{}^{Y}O_{-1}$. In the more heterogeneous Mic II, substitution (3) $^{A}Ca^{Y}O^{A}\square_{-1}{}^{Y}\square_{-1}$ is identical with secondary hydrothermal alteration of microlite (Lumpkin *et al.*, 1986, Novák and Černý, 1998; Geisler *et al.*, 2004; De Vito *et al.*, 2006; Loun *et al.*, 2018). Heterogeneous Ca-, F-rich Mic III has an unusual composition and the relevant substitution (4) $^{A}Ca_{0.5}{}^{Y}F_{0.5}{}^{Y}(OH)_{0.5}{}^{A}\square_{-0.5}{}^{Y}\square_{-1}$ is unique. It evidently demonstrates high activity of Ca and F in fluids which facilitated the crystallisation of Mic III, fersmite and of a distal Mic IIId on cracks of K-feldspar and quartz (Fig. 9). Substitution (4) clearly requires input of Ca and F from the external fluids, possibly from an amphibolite–biotite gneiss host (see below).

## Raman spectroscopy of microlite and textural features of metamictisation

Factor group analysis yields six Raman-active modes for microlite using the site symmetries $D_{3d}$ for *A* (16*d*) and *B* (16*c*) ions, $C_{2v}$ for *X* (48*f*) ions and $T_d$ for *Y* (8*b*) ions, respectively (Oliveira *et al.*, 2004). Only one Raman-active vibration is associated with the *Y*-site (8*b*) ions ($F_{2g}$) and five for the *X*-site (48*f*) ions ($A_g + E_g + 3F_{2g}$) (Glerup *et al.*, 2001). A tentative assignment of observed Raman modes was based on previous studies on pyrochlore-supergroup minerals (Geisler *et al.*, 2004; Oliveira *et al.*, 2004; Arenas *et al.*, 2010; Andrade *et al.*, 2013). However, the Raman shift of Mic I and II from Schinderhübel I is relatively different to the published data. Some of the bands are absent and most of the assigned bands were only roughly fitted. These Raman spectra display very broad, almost unrecognisable bands, suggesting very low structural order of Mic I and II (Fig. 10). Only Mic III provided spectra with relatively narrower and better-defined bands (mostly 532 and 637 $cm^{-1}$, which are absent in Mic I, II), similar to published microlite Raman spectra (Geisler *et al.*, 2004; Andrade *et al.*, 2013). Only two spectra demonstrated the presence of low-intensity $(OH)^{-}$ bands: spectrum 2 of Mic I with 3502 $cm^{-1}$ and spectrum 5 of Mic III with 3592 $cm^{-1}$ (Fig. 10b; Table 6). No O–H band was determined in predominantly altered domains of Mic II veinlets; $H_2O$ bands at 1630 $cm^{-1}$

https://doi.org/10.1180/mgm.2021.58 Published online by Cambridge University Press

**Table 5.** Representative compositions of microlite (Mic) and pyrochlore (Pcl) from Scheibengraben and Bienergraben.*

| Sample<br>No. anal. (type) | Sch 3<br>26 (Mic III) | Sch 2<br>27 (Mic III) | Sch 3<br>1 (Mic IIId) | Sch 3<br>3 (Mic IIId) | Bn 1<br>28 (Pcl III) | BN 3<br>21 (Mic III) | Bn 1<br>22 (Mic III) | Bn 3<br>23 (Mic III) |
|---|---|---|---|---|---|---|---|---|
| Element oxide contents (wt.%) | | | | | | | | |
| $WO_3$ | 0.45 | 0.14 | 0.10 | 0.07 | 0.10 | 0.21 | 0.14 | 0.20 |
| $Nb_2O_5$ | 5.95 | 6.64 | 4.73 | 4.94 | 35.78 | 9.83 | 14.20 | 9.93 |
| $Ta_2O_5$ | 70.19 | 61.03 | 58.91 | 58.75 | 47.41 | 67.30 | 61.72 | 67.28 |
| $SiO_2$ | – | 2.26 | 4.01 | 3.42 | – | – | – | – |
| $TiO_2$ | 0.72 | 2.33 | 2.37 | 2.76 | 0.93 | 1.92 | 1.24 | 1.79 |
| $ZrO_2$ | 0.20 | 0.18 | 0.25 | 0.20 | 0.17 | 0.08 | 0.47 | 0.12 |
| $UO_2$ | 0.20 | 0.83 | 0.76 | 1.01 | 0.32 | 0.69 | 0.20 | 0.60 |
| $Al_2O_3$ | – | 0.23 | 0.38 | 0.35 | – | – | – | – |
| $Sc_2O_3$ | – | – | – | – | – | – | – | 0.05 |
| $Ce_2O_3$ | 0.15 | 0.17 | 0.10 | 0.10 | 0.24 | 0.10 | 0.13 | 0.15 |
| $Sb_2O_3$ | – | 0.47 | 0.31 | 0.32 | – | – | – | – |
| FeO | 0.79 | 0.66 | 0.90 | 0.78 | 0.25 | 0.07 | 0.38 | 0.07 |
| MnO | 0.67 | 0.50 | 0.46 | 0.40 | 0.53 | 0.19 | 0.38 | 0.20 |
| SnO | – | 1.12 | 0.94 | 0.95 | – | – | – | – |
| CaO | 16.34 | 14.57 | 14.69 | 14.83 | 13.58 | 15.57 | 17.99 | 15.72 |
| $Na_2O$ | 0.98 | 1.70 | 1.31 | 1.37 | – | 1.89 | 0.36 | 1.71 |
| $F^-$ | 0.80 | 1.17 | 1.34 | 1.40 | – | 0.92 | 0.21 | 0.85 |
| $-O=F_2$ | −0.34 | −0.49 | −0.56 | −0.59 | – | −0.39 | −0.09 | −0.36 |
| Total | 97.10 | 93.51 | 91.01 | 91.07 | 99.31 | 98.37 | 97.34 | 98.33 |
| Element contents in atoms per formula unit (apfu) | | | | | | | | |
| $U^{4+}$ | 0.004 | 0.015 | 0.014 | 0.019 | 0.005 | 0.013 | 0.004 | 0.011 |
| $Sc^{3+}$ | | | | | 0.002 | | | 0.004 |
| $Ce^{3+}$ | 0.006 | 0.005 | 0.002 | 0.003 | 0.006 | 0.003 | 0.004 | 0.005 |
| $Sb^{3+}$ | | 0.016 | 0.010 | 0.011 | | | | |
| $Fe^{2+}$ | 0.117 | 0.046 | 0.061 | 0.054 | 0.028 | 0.010 | 0.052 | 0.010 |
| $Mn^{2+}$ | 0.050 | 0.035 | 0.032 | 0.028 | 0.030 | 0.013 | 0.026 | 0.014 |
| $Sn^{2+}$ | | 0.042 | 0.034 | 0.035 | | | | |
| $Ca^{2+}$ | 1.554 | 1.298 | 1.282 | 1.308 | 0.974 | 1.374 | 1.580 | 1.390 |
| $Na^+$ | 0.169 | 0.274 | 0.207 | 0.219 | 0.002 | 0.302 | 0.057 | 0.274 |
| Total *A* | 1.900 | 1.731 | 1.642 | 1.677 | 1.046 | 1.715 | 1.723 | 1.708 |
| $W^{6+}$ | 0.010 | 0.003 | 0.002 | 0.001 | 0.002 | 0.004 | 0.003 | 0.004 |
| $Nb^{5+}$ | 0.239 | 0.250 | 0.174 | 0.184 | 1.083 | 0.366 | 0.526 | 0.370 |
| $Ta^{5+}$ | 1.694 | 1.383 | 1.305 | 1.319 | 0.863 | 1.507 | 1.376 | 1.509 |
| $Si^{4+}$ | | 0.188 | 0.327 | 0.282 | | | | |
| $Ti^{4+}$ | 0.048 | 0.146 | 0.145 | 0.171 | 0.047 | 0.119 | 0.076 | 0.111 |
| $Zr^{4+}$ | 0.009 | 0.007 | 0.010 | 0.008 | 0.006 | 0.003 | 0.019 | 0.005 |
| $Al^{3+}$ | | 0.023 | 0.036 | 0.034 | | | | 0.002 |
| Total *B* | 2.000 | 2.000 | 1.999 | 1.999 | 2.001 | 1.999 | 2.000 | 2.001 |
| $F^-$ | 0.225 | 0.308 | 0.345 | 0.365 | | 0.240 | 0.054 | 0.222 |
| $O^{2-}$ | 6.679 | 6.271 | 6.092 | 6.143 | 6.028 | 6.400 | 6.631 | 6.417 |
| Total cations | 3.900 | 3.731 | 3.641 | 3.676 | 3.047 | 3.714 | 3.723 | 3.709 |
| Total anions | 6.904 | 6.579 | 6.437 | 6.508 | 6.028 | 6.640 | 6.685 | 6.639 |
| Nb# | 12.1 | 14.1 | 10.7 | 11.0 | 54.3 | 18.4 | 26.6 | 18.6 |
| Ta# | 85.5 | 77.7 | 80.4 | 78.8 | 43.3 | 75.7 | 69.6 | 75.8 |
| Ti# | 2.4 | 8.2 | 8.9 | 10.2 | 2.4 | 6.0 | 3.8 | 5.6 |
| Ta/(Ta+Nb) | 0.88 | 0.85 | 0.88 | 0.88 | 0.44 | 0.80 | 0.72 | 0.80 |

* '–' content of the element is below detection limit. Abbreviations: Sch – Scheibengraben, Bn – Bienergraben. *A*-, *B* – structural positions of pyrochlore structure. Mic III, IIId, Pcl III – microlite (Pcl – pyrochlore) types and at individual pegmatites. End-members of pyrochlore supergroup minerals (molecule %): pyrochlore (Nb#), microlite (Ta#) and betafite (Ti#).

are absent. These differences could be attributed to aqueous alteration (Geisler *et al.*, 2004), though more probably result from the radiation damage (Zietlow, 2016; Zietlow *et al.*, 2017) due to the high U content (≤23 wt.%) in Mic I and Mic II, whereas it is below 4.5 wt.% in Mic III and IIId.

In addition to compositional variations, extensive textural transformations (existence of haloes surrounding metamict grains, high microporosity, etc.) are the most prominent markers of alteration and recrystallisation of the microlite crystals. Such textural variations are best seen in Mic I–III from Schinderhübel I (Fig. 3): homogeneous to slightly oscillatory zoned Mic I is characterised by a high porosity and extensive fracturing of its grain relics. Cracks in Mic I are filled by irregularly zoned Mic II veinlets (Fig. 3a,b). Finally, homogeneous-to-oscillatory zoned U-poor Mic III exhibits a low porosity and radiation damage. Radioactive decay of α particles of suitable radionuclides (especially U and Th) and recoil nuclei processes lead to amorphisation of the microlite structure (Ewing, 1994; Ewing *et al.*, 2000; Zietlow, 2016; Zietlow *et al.*, 2017), which is manifested by an increase in grain volume and radial cracks from the core to the grain periphery (Lee and Tromp, 1995; Loun *et al.*, 2018).

## Fluid-mediated alteration of microlites

Several alteration and recrystallisation stages of microlite were recognised, mainly in the Schinderhübel I pegmatite: (1) formation of Mic I on CGM fractures; (2) recrystallisation of Mic I on Mic II; and (3) recrystallisation/replacement of both Mic I and II on Mic III. Microlite I has a slightly low *A*-site vacancy,

https://doi.org/10.1180/mgm.2021.58 Published online by Cambridge University Press

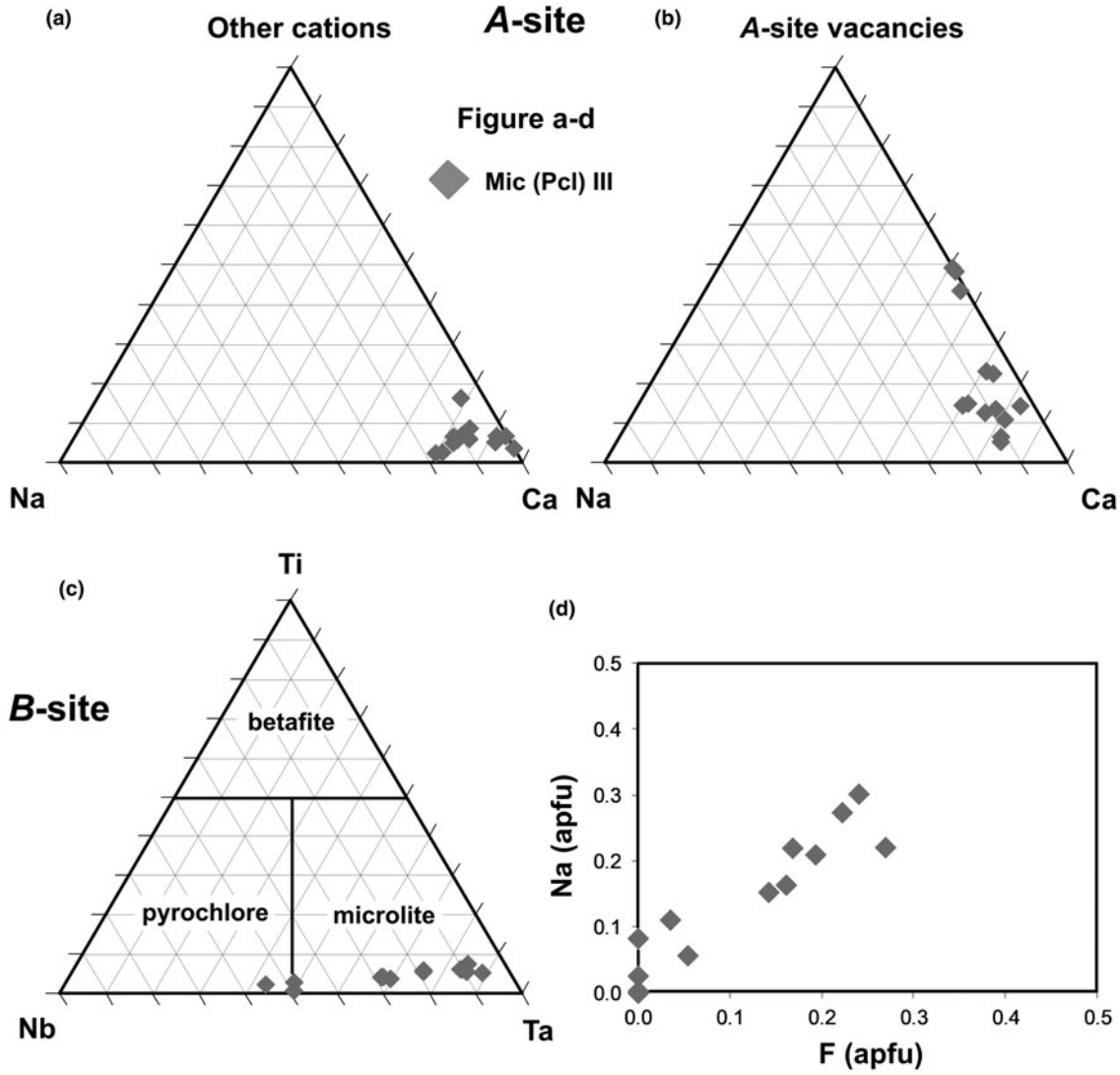


**Fig. 8.** Ternary classification diagrams and F-Na plot for microlites and pyrochlore in Bienergraben: (a) *A*-site (Na–Ca–other cations); (b) *A*-site (Na–Ca–vacancy); (c) *B*-site (Nb–Ta–Ti); (d) F versus Na plot. Note, 'Other cations' represent Th, Sb, Sc, Ce, Fe, Mn and Sn in the *A*-site.

moderate contents of Na (≤0.40 apfu) and very low F. The microlite I composition was probably more or less modified during the subsequent stage (2), characterised by a significant increase in the *A*-site vacancy (Fig. 6b). Loss of Na and Ca are typical whereas *B*-site cations as well as concentrations of U are stable (Figs 6c, 9). This indicates resistance of U during early replacement processes and does not fully correlate with the common U loss described in altered metamict microlite (e.g. Ewing *et al.*, 2000; Zietlow *et al.*, 2017). Substantial *A*-site cation loss is marked by a decrease in analytical totals in Mic II to ~90 wt.%. Both (1) and (2) stages might represent individual episodes of generally assumed secondary alteration in granitic pegmatites in the sense of Lumpkin and Ewing (1992). In contrast to stages (1) and (2), stage (3) includes more complex compositional variations. Mineral-replacement processes lead to Na and predominantly U and Ti loss, as well as evident Ca- and F-enrichments (Figs 6a,b,d, 9).

The origin of early Mic I was probably facilitated by residual fluids exsolved from pegmatite melt in the latest stage of magmatic crystallisation. However, some participation of externally derived fluids is indicated by the elevated Mg contents of the associated recrystallised CGM (Chládek *et al.*, 2020). The chemical signature of this later process is transitional between primary magmatic microlite and the microlite originated during early alteration (Lumpkin and Ewing, 1992). The fluids that generated Mic II could have a similar origin as those forming Mic I, although the alteration proceeded at slightly lower temperatures along thin cracks in the CGM (Fig. 3a,b). This compositional trend resulted in an increased *A*-site vacancy in Mic II; and is similar to the secondary alteration defined by Lumpkin and Ewing (1992), and described from numerous pegmatites (e.g. Chudík and Uher, 2009; Chudík *et al.*, 2011; Melcher *et al.*, 2015; Loun *et al.*, 2018). However, the microlite compositions with very high *A*-site vacancy and very low contents of F, typical for low-temperature hydrothermal and weathering processes facilitated by meteoritic fluids (e.g. Lumpkin and Ewing, 1992; Loun *et al.*, 2018), are absent in the pegmatites investigated.

The latest stage of microlite, Mic III (+ IIId), characterised by high Ca, low *A*-site vacancy and elevated F contents does not fit

https://doi.org/10.1180/mgm.2021.58 Published online by Cambridge University Press

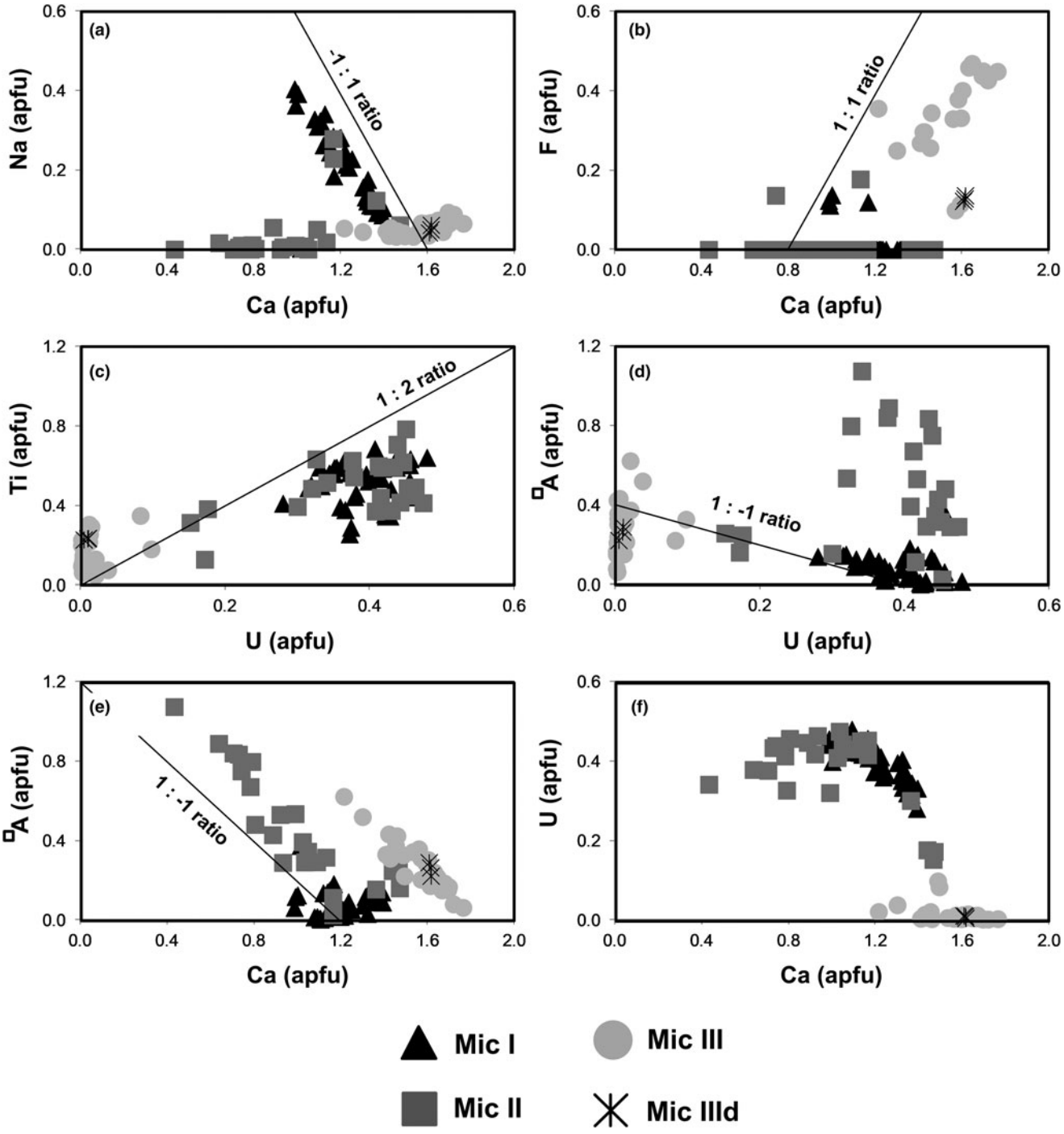


**Fig. 9.** Correlations of elemental concentrations in atoms per formula unit (apfu) in Mic I–III and IIId from Schinderhübel I: (a) Ca *vs*. Na; (b) Ca *vs*. F; (c) U *vs*. Ti; (d) U *vs*. vacancy in the *A*-site; (e) Ca *vs*. vacancy in the *A*-site; (f) Ca *vs*. U.

with final low-temperature secondary alteration of pyrochlore-supergroup minerals described elsewhere (e.g. Lumpkin and Ewing, 1992; Llorens and Moro, 2010; Loun *et al.*, 2018). A significant addition of Ca is apparent in the fluids from the Schinderhübel I pegmatite, demonstrated by the common association of epidote ± pumpellyite (Dostál, 1966; unpubl. data of MN) with late pyrochlore (Novák and Dosbaba, 2006), and by secondary bavenite–bohseite after beryl, known from most Maršíkov pegmatites (Dolníček *et al.*, 2020a,b). Whether there is an external or internal source of Ca in subsolidus processes in granitic pegmatites is a matter of discussion, and an external source has been suggested (e.g. Martin and De Vito, 2014; Novák *et al.*, 2017). Further, the temperature of these external fluids might be slightly higher relative to stage (2). Fissure-filling Mic III (+ IIId) texturally resembles Alpine-type hydrothermal veins (e.g. Weisenberger and Bucher, 2011) and these authors also consider host rocks the sourcee, not only of Ca, but also other elements. Consequently, late hydrothermal-metamorphic fluids could facilitate the origin of Mic III, Mic IIId and associated fersmite (Fig. 3). Fluorine might have been released from the rock-forming

https://doi.org/10.1180/mgm.2021.58 Published online by Cambridge University Press

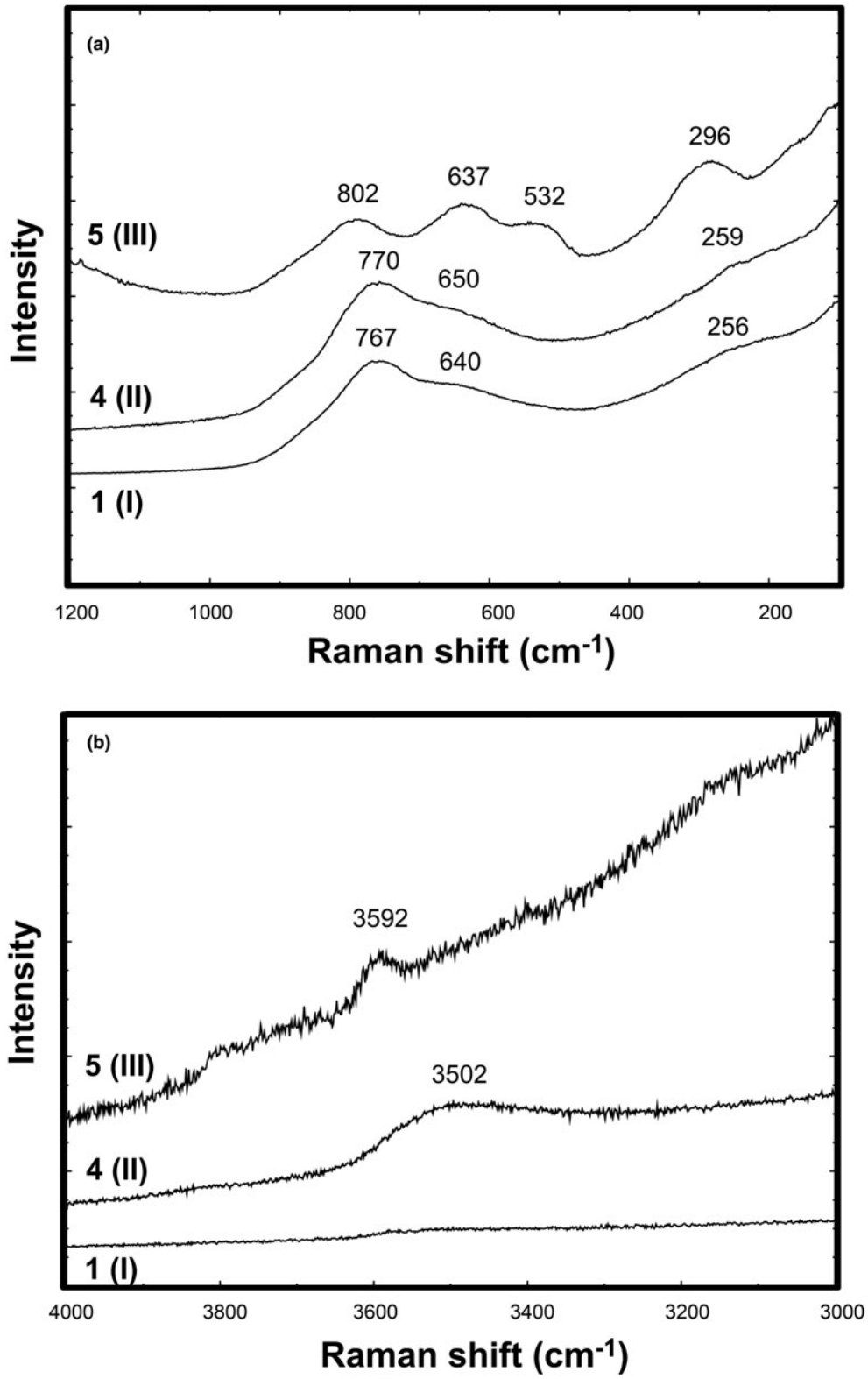


**Fig. 10.** Representative Raman spectra of Mic I–III from Schinderhübel I: (a) 100–1200 $cm^{-1}$ region; (b) 3000–4000 $cm^{-1}$ region; abbreviation: 1 (I) is number of analysis (microlite type).

minerals of the host amphibole gneiss or parental pegmatite during such a hydrothermal-metamorphic overprint. Biotite and amphibole from host rocks are potential sources of fluorine; elevated concentrations of fluorine were found in pumpellyite (≤0.45 wt.% F) and epidote (≤0.2 wt.% F) associated with bavenite–bohseite at thin Alpine-type veinlets cutting the Schinderhübel I pegmatite (unpubl. data of MN). However, we cannot exclude pegmatitic muscovite (≤0.2 wt.% F; Dolníček *et al.*, 2020b) as another source of F.

https://doi.org/10.1180/mgm.2021.58 Published online by Cambridge University Press

**Table 6.** Raman bands and their assignments in Mic I, II and III from Schinderhübel I pegmatite (in $cm^{-1}$) compared to unaltered microlite from Geisler *et al.* (2004).*

| Vibration | Mode | 1 (Mic I) | 2 (Mic I) | 3 (Mic I) | 4 (Mic II) | 5 (Mic III) | 6 (Mic III) | Geisler *et al.* (2004) |
|---|---|---|---|---|---|---|---|---|
| *A–Y* stretching + X–A–Y bending | $T_{2g}$ | 256 | 258 | 251 | 259 | | | 248 |
| *X–B–X* bending | $E_g$ | | | | | 296 | 286 | 302 |
| *X–B–X* bending | $E_g$ | | | | | | | 338 |
| *B–X* octahedra stretching | $A_{1g}$ | | | | | 532 | 540 | 549 |
| *B–X* octahedra stretching | $T_{2g}$ | 640 | 645 | 629 | 650 | 637 | 637 | 637 |
| Vibrational mode in amorphous structure (?) | $T_{2g}$ | 767 | 765 | 772 | 770 | 802 | 800 | 800 |
| $(OH)^-$ | | | 3502 | | | 3592 | | |

*Abbreviation: 1 (Mic I) – analysis (microlite type).

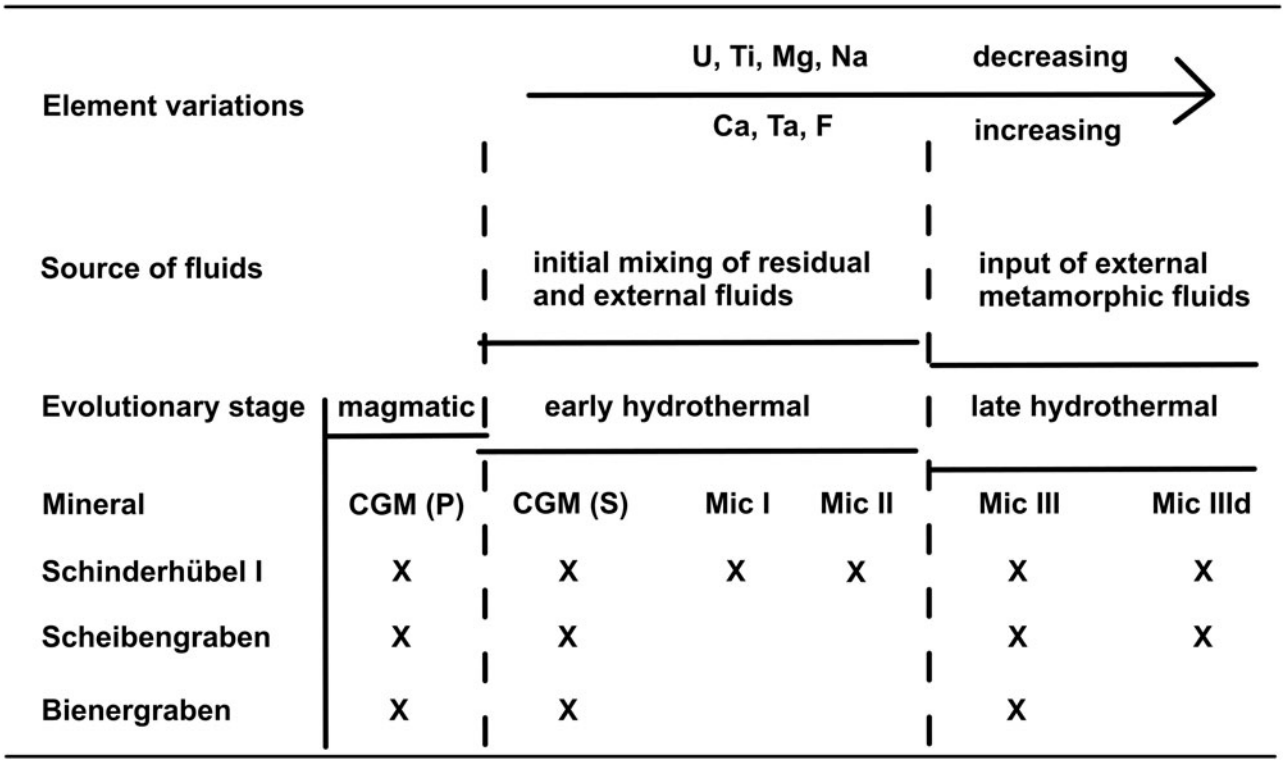


**Fig. 11.** Evolutionary sequence of microlite-group minerals.

## Conclusions

Microlite- (and rarely pyrochlore-) group minerals are essential tracers of post-magmatic evolution of the beryl–columbite pegmatites in the Maršíkov District. Complex subsolidus evolution of Nb–Ta mineralisation involves individual stages (1), (2) and (3) producing microlite types [Mic I, Mic II, Mic III and Mic IIId], respectively (Fig. 11). The complete sequence of microlite types has only been found in the Schinderhübel I pegmatite. The alteration processes commenced with recrystallisation of primary magmatic to secondary post-magmatic CGM, facilitated by residual fluids locally mixed with external fluids from the host rocks (Chládek *et al.*, 2020) and crystallisation of early Na-rich Mic I. Subsequent formation of Na-poor Mic II indicates a change of the fluid composition connected with partial alteration of Mic I and removal of Na (Fig. 11). Microlite II is compositionally very similar to secondary alteration microlite (*sensu* Lumpkin and Ewing, 1992). The latest stage (3), producing Ca- and F-enriched Mic III + fersmite and rare distal Mic IIId displays a different textural style; hence, the extensive introduction of external (metamorphic) fluids enriched in Ca, and perhaps F is feasible. The wide diversity of compositional and textural features of microlite minerals and secondary CGM reflects the complex evolution of the pegmatites during the subsolidus, late hydrothermal stage, probably including a weak-to-moderate metamorphic overprint at the latest event.

**Acknowledgements.** We thank Alessandro Guastoni, Magdalena Dumańska-Słowik, an anonymous reviewer and editors of the *Mineralogical Magazine* for their critical and constructive reviews, as well as Viera Kollárová for their assistance during electron microprobe work. This research was supported by the Slovak Research and Development Agency (APVV-15-0050 and APVV-18-0065 projects), the Ministry of Education, Slovak Republic (VEGA-1/0499/16, VEGA-1/007915 and VEGA-1/0137/20) to PU and PB, the research project GAČR 19-05198S to MN, the Ministry of Education, Youth and Sports of the Czech Republic, Grant number SGS SP 2020/105 to ŠCH and by the Palacký University in Olomouc (IGA_PrF_2020_030) to TO.

## References

Amores-Casals S., Gonçalves A.O., Melgarejo J.C. and Martí J. (2020) Nb and REE Distribution in the Monte Verde Carbonatite–Alkaline–Agpaitic Complex (Angola). *Minerals*, **10**, 5.

Andrade M.B., Atencio D., Chukanov N.V. and Ellena J. (2013) Hydrokenomicrolite, $(\square,H_2O)_2Ta_2(O,OH)_6(H_2O)$, a new microlite group mineral from Volta Grande pegmatite, Nazareno, Minas Gerais, Brazil. *American Mineralogist*, **98**, 292–296.

Andrade M.B., Yang H., Atencio D., Downs R.T., Chukanov N.V., Lemée-Cailleau M.H., Persiano A.I.C., Goeta A.E. and Ellena J. (2017) Hydroxylcalciomicrolite, $Ca_{1.5}Ta_2O_6(OH)$, a new member of the microlite group from Volta Grande pegmatite, Nazareno, Minas Gerais, Brazil. *Mineralogical Magazine*, **81**, 555–564.

Arenas D.J., Gasparov L.V., Qiu W., Nino J.C., Patterson C.H. and Tanner D.B. (2010) Raman study of phonon modes in bismuth pyrochlores. *Physical Review*, **82**, 214302.

Atencio D., Andrade M.B., Christy A.G., Gieré R. and Kartashov P.M. (2010) The pyrochlore supergroup of minerals: Nomenclature. *The Canadian Mineralogist*, **48**, 673–698.

Atencio D., Andrade M.B., Neto A.C.B. and Pereira V.P. (2017) Ralstonite renamed hydrokenoralstonite, coulsellite renamed fluornatrocoulsellite, and their incorporation into the pyrochlore supergroup. *The Canadian Mineralogist*, **55**, 115–120.

Atencio D., Andrade M.B., Bindi L., Bonazzi P., Zoppi M., Stanley C.J. and Kristiansen R. (2018) Kenoplumbomicrolite, $(Pb,\square)_2Ta_2O_6[\square,(OH),O]$, a new mineral from Ploskaya, Kola Peninsula, Russia. *Mineralogical Magazine*, **82**, 1049–1055.

Bonazzi P., Bindi L., Zoppi M., Capitani G.C. and Olmi F. (2006) Single-crystal diffraction and transmission electron microscopy studies of "silicified" pyrochlore from Narssârssuk, Julianehaab district, Greenland. *American Mineralogist*, **91**, 794–801.

Čech F. (1973) Manganoan tapiolite from Northern Moravia, Czechoslovakia. *Acta Universitatis Carolinae, Geologica*, **1–2**, 37–45.

Černý P. and Ercit T.S. (2005) The classification of granitic pegmatites revisited. *The Canadian Mineralogist*, **43**, 2005–2026.

Černý P., Novák M. and Chapman R. (1992) Effects of sillimanite-grade metamorphism and shearing on Nb,Ta-oxide minerals in granitic pegmatites: Maršíkov, northern Moravia, Czechoslovakia. *The Canadian Mineralogist*, **30**, 699–718.

Černý P., Novák M. and Chapman R. (1995) The Al (Nb,Ta) $Ti_{-2}$ substitution in titanite: the emergence of a new species? *Mineralogy and Petrology*, **52**, 61–73.

Cháb J., Fediuková E., Fišera M., Novotný P. and Opletal M. (1990) Variscan orogeny in the Silesicum (ČSFR). *Sborník geologických věd, Ložisková geologie a mineralogie*, **29**, 9–39 [in Czech, English summary].

Cháb J., Stráník Z. and Eliáš M. (2007) *Geological map of the Czech Republic 1 : 500000*. Czech Geological Survey, Prague, Czech Republic [in Czech, English summary].

Chakhmouradian A.R. and Mitchell R.H. (2002) New data on pyrochlore- and perovskite-group minerals from the Lovozero alkaline complex, Russia. *European Journal of Mineralogy*, **14**, 821–836.

Chládek Š., Uher P. and Novák M. (2020) Compositional and textural variations of columbite-group minerals from beryl-columbite pegmatites, the Maršíkov District, Bohemian Massif, Czech Republic: magmatic *versus* hydrothermal evolution. *The Canadian Mineralogist*, **58**, 767–783.

Christy A.G. and Atencio D. (2013) Clarification of status of species in the pyrochlore supergroup. *Mineralogical Magazine*, **77**, 13–20.

Chudík P. and Uher P. (2009) Pyrochlore group minerals from the granitic pegmatites of the Western Carpathians: Compositional variations and substitution mechanisms. *Mineralia Slovaca*, **41**, 159–168 [in Slovak with English summary].

Chudík P., Uher P., Gadas P., Škoda R. and Pršek J. (2011) Niobium-tantalum oxide minerals in the Jezuitské Lesy granitic pegmatite, Bratislava Massif, Slovakia: Ta to Nb and Fe to Mn evolutionary trends in a narrow Be, Cs-rich and Li,B-poor dike. *Mineralogy and Petrology*, **102**, 15–27.

Demartis M., Melgarejo J.C., Colombo F., Alfonso P., Coniglio J.E., Pinotti L.P. and D'Eramo F.J. (2014) Extreme F activities in late pegmatitic events as a key factor for LILE and HFSE enrichment: the Ángel pegmatite, Central Argentina. *The Canadian Mineralogist*, **52**, 247–269.

De Vito C.D., Pezzotta F., Ferrini V. and Aurisicchio C. (2006) Nb–Ta–Ti oxides in the gem-mineralized and "hybrid" Anjanabonoina granitic pegmatite, Central Madagascar: a record of magmatic and postmagmatic events. *The Canadian Mineralogist*, **44**, 87–103.

Dey M., Mitchell R.H., Bhattacharjee S., Chakrabarty A., Pal S., Pal S. and Sen A.K. (2021) Composition and genesis of albitite-hosted antecrystic pyrochlore from the Sevattur carbonatite complex, India. *Mineralogical Magazine*, **85**, 568–587.

Dolníček Z., Nepejchal M., Sejkora J., Ulmanová J. and Chládek Š. (2020a) Bohseite from beryl-columbite pegmatite D6e in Maršíkov (Silesicum, Czech Republic). *Bulletin Mineralogie Petrologie*, **28**, 219–223 [in Czech with English summary].

Dolníček Z., Nepejchal M. and Novák M. (2020b) Minerals of the bavenite-bohseite series from the Schinderhübel I pegmatite in Maršíkov (Silesicum, Czech Republic). *Bulletin Mineralogie Petrologie*, **28**, 353–358 [in Czech with English summary].

Dostál J. (1966) Mineralogische und Petrographische Verhältnisse von Chrysoberyll-Sillimanit Pegmatit von Maršíkov. *Acta Universitatis Carolinae, Geologica*, **4**, 271–287.

Dumańska-Slowik M., Pieczka A., Tempesta G., Olejniczak Z. and Heflik W. (2014) "Silicified" pyrochlore from nepheline syenite (mariupolite) of the Mariupol Massif, SE Ukraine: A new insight into the role of silicon in the pyrochlore structure. *American Mineralogist*, **99**, 2008–2017.

Duran Ch.J., Seydoux-Guillaume A.M., Bingen B., Gouy S., De Parseval P., Ingrin J. and Guillaume D. (2016) Fluid-mediated alteration of (Y,REE,U, Th)–(Nb,Ta,Ti) oxide minerals in granitic pegmatite from the Evje-Iveland district, southern Norway. *Mineralogy and Petrology*, **110**, 581–599.

Ercit T.S. (1994) The geochemistry and crystal chemistry of columbite-group minerals from granitic pegmatites, southwestern Grenville Province, Canadian Shield. *The Canadian Mineralogist*, **32**, 421–438.

Ewing R.C. (1975) The crystal chemistry of complex niobium and tantalum oxides. IV. The metamict state: Discussion. *American Mineralogist*, **60**, 728–733.

Ewing R.C. (1994) The metamict state: 1993 the centennial. *Nuclear Instruments and Methods in Physics Research*, **B91**, 22–29.

Ewing R.C., Meldrum A., Wang L.M. and Wang S.X. (2000) Radiation-induced amorphisation. Pp. 319–362 in: *Transformation Processes in Minerals* (R.C. Ewing, A. Meldrum, L.M. Wang and S.X. Wang, editors). Reviews in Mineralogy and Geochemistry, **39**. Mineralogical Society of America, Washington DC.

Franz G. and Morteani G. (1984) The formation of chrysoberyl in metamorphosed pegmatites. *Journal of Petrology*, **25**, 27–52.

Galliski M.Á., Márquez-Zavalía M.F., Černý P. and Lira R. (2016) Complex Nb-Ta-Ti-Sn oxide mineral intergrowths in the La Calandria pegmatite, Cañada del Puerto, Córdoba, Argentina. *The Canadian Mineralogist*, **54**, 899–916.

Geisler T., Berndt J., Meyer H.W., Pollok K. and Putnis A. (2004) Low-temperature aqueous alteration of crystalline pyrochlore: correspondence between Nature and experiment. *Mineralogical Magazine*, **68**, 905–922.

Glerup M., Nielsen O.F. and Poulsen F.W. (2001) The structural transformation from the pyrochlore structure, $A_2B_2O_7$, to the fluorite structure, $AO_2$, studied by Raman spectroscopy and defect chemistry modeling. *Journal of Solid State Chemistry*, **160**, 25–32.

Gonçalves A.O., Melgarejo J.C., Alfonso P., Amores S., Paniagua A., Neto A.B., Morais E.A. and Camprubí A. (2019) The distribution of rare metals in the LCT pegmatites from the Giraúl Field, Angola. *Minerals*, **9**, 1–38.

Guastoni A., Diella V. and Pezzotta F. (2008) Vigezzite and associated oxides of Nb-Ta from emerald bearing pegmatites of the Vigezzo valley (Western Alps, Italy). *The Canadian Mineralogist*, **46**, 783–797.

Hegner E. and Kröner A. (2000) Review of Nd isotopic data and xenocrystic and detrital zircon ages from the pre-Variscan basement in the eastern Bohemian Massif: speculations on palinspatic reconstruction. Pp. 113–129 in: *Orogenic Processes: Quantification and Modelling in the Variscan Belt* (W. Franke, V. Haak, O. Oncken and D. Tanner, editors). Geological Society, Special Publications, Vol. 179. London, UK.

Hogarth D.D. (1977) Classification and nomenclature of the pyrochlore group. *American Mineralogist*, **62**, 403–410.

Janoušek V., Aichler J., Hanžl P., Gerdes A., Erban V., Žáček V., Pecina V., Pudilová M., Hrdličková K., Mixa P. and Žáčková E. (2014) Constraining genesis and geotectonic setting of metavolcanic complexes: a multidisciplionary study of the Devonian Vrbno Group (Hrubý Jeseník Mts., Czech Republic). *International Journal of Earth Sciences*, **103**, 455–483.

https://doi.org/10.1180/mgm.2021.58 Published online by Cambridge University Press

Johan V. and Johan Z. (1994) Accessory minerals of the Cínovec (Zinnwald) granite cupola, Czech Republic Part 1: Nb-, Ta-, and Ti-bearing oxides. *Mineralogy and Petrology*, **51**, 323–343.

Kasatkin A.V., Britvin S.N., Peretyazhko I.S., Chukanov N.V., Škoda R. and Agakhanov A.A. (2020) Oxybismutomicrolite, a new pyrochlore-supergroup mineral from the Malkhan pegmatite field, Central Transbaikalia, Russia. *Mineralogical Magazine*, **84**, 444–454.

Košuličová M. and Štípská P. (2007) Variations in the transient prograde geothermal gradient from chloritoid-staurolite equilibria: a case study from the Barrovian and Buchan-type domains in the Bohemian Massif. *Journal of Metamorphic Geology*, **25**, 19–36.

Krönner A., O´Brien P.J., Nemchin A.A. and Pidgeon R.T. (2000) Zircon ages for high pressure granulites from South Bohemia, Czech Republic, and their connection to Carboniferous high temperature processes. *Contributions to Mineralogy and Petrology*, **138**, 127–142.

Kruťa T. (1966) *Moravian Minerals and their Literature 1940–1965*. Moravské museum, Brno, 379 pp [in Czech, English summary].

Laurent A., Janoušek V., Magna T., Schulmann K. and Míková J. (2014) Petrogenesis and geochronology of a post-orogenic calc-alkaline magmatic association: the Žulová Pluton, Bohemian Massif. *Journal of Geosciences*, **59**, 415–440.

Lee J.K.W. and Tromp J. (1995) Self-induced fracture generation in zircon. *Journal of Geophysical Research*, **B9**, 17753–17770.

Llorens T. and Moro M.C. (2010) Microlite and tantalite in the LCT granitic pegmatites of La Canalita, Navasfrías Sn–W District, Salamanca, Spain. *The Canadian Mineralogist*, **57**, 155–171.

Loun J., Novák M., Cempírek J., Škoda R., Vašinová–Galiová M., Prokeš L., Dosbaba M. and Čopjaková R. (2018) Geochemistry and secondary alterations of microlite from eluvial deposits in the Numbi mining area, S. Kivu, Democratic Republic of the Congo. *The Canadian Mineralogist*, **56**, 1–18.

Lumpkin G.R. (1998) Rare-element mineralogy and internal evolution of the Rutherford #2 pegmatite, Amelia County, Virginia: a classic locality revisited. *The Canadian Mineralogist*, **36**, 339–353.

Lumpkin G.R. and Ewing R.C. (1992) Geochemical alteration of pyrochlore group minerals: Microlite subgroup. *American Mineralogist*, **77**, 179–188.

Lumpkin G.R. and Ewing R.C. (1996) Geochemical alteration of pyrochlore group minerals: Betafite subgroup. *American Mineralogist*, **81**, 1237–1248.

Lumpkin G.R., Chakoumakos B.C. and Ewing R.C. (1986) Mineralogy and radiation effects of microlite from the Harding pegmatite, Taos County, New Mexico. *American Mineralogist*, **71**, 569–588.

Lumpkin G.R., Gieré R., Williams C.T., McGlinn P.J. and Payne T.E. (2017) Petrography and chemistry of tungsten-rich oxycalciobetafite in hydrothermal veins of the Adamello contact aureole, northern Italy. *Mineralogy and Petrology*, **111**, 499–509.

Martin R.F. and De Vito C.D. (2014) The late-stage miniflood of Ca in granitic pegmatites: an open-system acid-reflux model involving plagioclase in the exocontact. *The Canadian Mineralogist*, **52**, 165–181.

Melcher F., Graupner T., Gäbler H.E., Sitnikova M., Henjes-Kunst F., Oberthür T., Gerdes A. and Dewaele S. (2015) Tantalum – (niobium – tin) mineralisation in African pegmatites and rare metal granites: Constraints from Ta – Nb oxide mineralogy, geochemistry and U – Pb geochronology. *Ore Geological Reviews*, **64**, 667–719.

Melgarejo J.C., Costanzo A., Bambi A.C.J.M., Gonçalves A.O. and Neto A.B. (2012) Subsolidus processes as a key factor on the distribution of Nb species in plutonic carbonatites: The Tchivira case, Angola. *Lithos*, **152**, 187–201.

Meyer C. and Young S.V. (1988) Tungsten-bearing yttrobetafite in lunar granophyre. *American Mineralogist*, **73**, 1420–1425.

Mikulski S.Z., Williams I.S. and Bagiński B. (2013) Early Carboniferous (Viséan) emplacement of the collisional Klodsko-Zloty Stok granitoids (Sudetes, SW Poland): constraints from geochemical data and zircon U–Pb ages. *International Journal of Earth Sciences*, **102**, 1007–1027.

Mokhov A.V., Kartashov P.M., Bogatikov O.A., Ashikhmina N.A., Magazina L.O. and Koporulina E.V. (2008) Fluorite, hatchettolite, calcium sulfate, and bastnasite-(Ce) in the lunar regolith from Mare Crisium. *Doklady Earth Sciences*, **422**, 1178–1180.

Nasdala L., Kronz A., Wirth R., Váczi T., Pérez-Soba C., Willner A. and Kennedy A.K. (2009) The phenomenon of deficient electron micro-probe totals in radiation-damaged and altered zircon. *Geochimica et Cosmochimica Acta*, **73**, 1637–1650.

Novák M. (1988) Garnets from pegmatites of the Hrubý Jeseník (northern Moravia). *Acta Musei Moraviae, Scientiae Naturales*, **73**, 3–28 [in Czech, English summary].

Novák M. (2005) Granitic pegmatites of the Bohemian Massif (Czech Republic); Mineralogical, geochemical and regional classification and geological significance. *Acta Musei Moraviae, Scientiae Geologicae*, **90**, 3–74 [in Czech, English summary].

Novák M. and Černý P. (1998) Niobium – tantalum oxide minerals from complex granitic pegmatites in the Moldanubicum, Czech Republic: primary versus secondary compositional trends. *The Canadian Mineralogist*, **36**, 659–672.

Novák M. and Dosbaba M. (2006) Breakdown of primary columbite–tantalite related to Alpine-type hydrothermal alteration, and redistribution of its components. *Acta Mineralogica-Petrographica, Abstract Series*, **5**, 85.

Novák M. and Rejl L. (1993) Relations of the muscovite pegmatites to the geophysical fields in the area of the HrubýJeseník Mts., Czechoslovakia. *Acta Musei Moraviae, Scientiae Naturales*, **77**, 49–61 [in Czech, English summary].

Novák M., Uher P., Černý P. and Siman P. (2000) Compositional variations in ferrotapiolite+tantalite pairs from the beryl-columbite pegmatite at Moravany nad Váhom, Slovakia. *Mineralogy and Petrology*, **69**, 295–306.

Novák M., Černý P. and Uher P. (2003) Extreme variation and apparent reversal of Nb-Ta fractionation in columbite-group minerals from the Scheibengraben beryl-columbite pegmatite, Maršíkov, Czech Republic. *European Journal of Mineralogy*, **15**, 565–574.

Novák M., Čopjaková R., Dosbaba M., Galiová M.V., Všianský D. and Staněk J. (2015) Two paragenetic types of cookeite from the Dolní Bory-Hatě pegmatites, Moldanubian Zone, Czech Republic: Proximal and distal alteration products of Li-bearing sekaninaite. *The Canadian Mineralogist*, **53**, 1035–1048.

Novák M., Prokop J., Losos Z. and Macek I. (2017) Tourmaline, an indicator of external Mg-contamination of granitic pegmatites from host serpentinite; examples from the Moldanubian Zone, Czech Republic. *Mineralogy and Petrology*, **111**, 625–641.

Oliveira E.A., Guedes I., Ayala A.P., Gesland J.Y., Ellena J., Moreira R.L. and Grimsditch M. (2004) Crystal structure and vibrational spectrum of the $NaCaMg_2F_7$ pyrochlore. *Journal of Solid State Chemistry*, **177**, 2943–2950.

Pokorný J. and Staněk J. (1951) Beryl pegmatite from Scheibengraben near Maršíkov. *Práce Moravskoslezské Akademie Věd Přírodních*, **7**, 247–258 [in Czech].

Pouchou J.L. and Pichoir F. (1985) "PAP" (phi-rho-z) procedure for improved quantitative microanalysis. Pp. 104–106 in: *Microbeam Analysis* (J.T. Armstrong, editors). San Francisco Press, San Francisco, USA.

Prol-Ledesma R.M., Melgarejo J.C. and Martin R.F. (2012) The El Muerto "NYF" granitic pegmatite, Oaxaca, Mexico, and its striking enrichment in allanite-(Ce) and monazite-(Ce). *The Canadian Mineralogist*, **50**, 1055–1076.

René M. (1983) Geochemistry and petrology of metapelites in the envelope of the core of the Desná Dome in northern Moravia. *Časopis pro Mineralogii a Geologii*, **28**, 277–286 [in Czech].

Schulmann K., Oliot E., Košuličová M., Montigny R. and Štípská P. (2014) Variscan thermal overprints exemplified by U–Th–Pb monazite and K–Ar muscovite and biotite dating at the eastern margin of the Bohemian Massif (East Sudetes, Czech Repubic). *Journal of Geosciences*, **59**, 389–413.

Sharygin V.V., Sobolev N.V. and Channer D.M.DeR. (2009) Oscillatory-zoned pyrochlore-group minerals from the Guaniamo kimberlites, Venezuela. *Lithos*, **112**, 976–985.

Siegel K., Vasyukova O.V. and Williams-Jones A.E. (2018) Magmatic evolution and controls on rare metal-enrichment of the Strange Lake peralkaline A-type granitic pluton, Québec-Labrador. *Lithos*, **308–309**, 34–52.

Spilde M.N. and Shearer C.K. (1992) A comparison of tantalum-niobium oxide assemblages in two mineralogically distinct rare-element granitic pegmatites, Black Hills, South Dakota. *The Canadian Mineralogist*, **30**, 719–737.

Szuszkiewicz A., Pieczka A., Szełęg E., Turniak K., Ilnicki S. and Nejbert K. (2016) The euxenite-group minerals and products of their alteration in the hybrid Julianna granitic pegmatite, Piława Górna, Sudetes, southwestern Poland. *The Canadian Mineralogist*, **54**, 879–898.

https://doi.org/10.1180/mgm.2021.58 Published online by Cambridge University Press

Tindle A.G. and Breaks F.W. (1998) Oxide minerals of the Separation Rapids rare-element granitic pegmatite group, northwestern Ontario. *The Canadian Mineralogist*, **36**, 609–635.

Uher P., Černý P., Chapman R., Határ J. and Miko O. (1998) Evolution of Nb, Ta-oxide minerals in the Prašivá granitic pegmatites, Slovakia. II. External hydrothermal overprint. *The Canadian Mineralogist*, **36**, 535–545.

Walter B.F., Parsapoor A., Braunger S., Marks M.A.W., Wenzel T., Martin M. and Markl G. (2018) Pyrochlore as a monitor for magmatic and hydrothermal processes in carbonatites from the Kaiserstuhl volcanic complex (SW Germany). *Chemical Geology*, **498**, 1–16.

Weisenberger T. and Bucher K. (2011) Mass transfer and porosity evolution during low temperature water–rock interaction in gneisses of the Simano nappe: Arvigo, Val Calanca, Swiss Alps. *Contributions to Mineralogy and Petrology*, **162**, 61–81.

Zaitsev A.N., Spratt J., Shtukenberg A.G., Zolotarev A.A., Britvin S.N., Petrov S.V., Kuptsova A.V. and Antonov A.V. (2021) Oscillatory- and sector-zoned pyrochlore from carbonatites of the Kerimasi volcano, Gregory rift, Tanzania. *Mineralogical Magazine*, **85**, 532–553.

Zietlow P. (2016) *Properties and Recrystallization of Radiation Damaged Pyrochlore and Titanite*. PhD dissertation, University of Hamburg, Germany.

Zietlow P., Beirau T., Mihailova B., Groat L.A., Chudy T., Shelyug A., Navrotsky A., Ewing R.C., Schlütter J., Škoda R. and Bismayer U. (2017) Thermal annealing of natural, radiation-damaged pyrochlore. *Zeitschrift fur Kristallographie*, **232**, 25–38.

https://doi.org/10.1180/mgm.2021.58 Published online by Cambridge University Press